

AD-A036 344

RENSSELAER POLYTECHNIC INST TROY N Y DEPT OF MECHANI--ETC F/G 20/11
NONLINEAR MONOTONIC FUNCTIONS WITH SELECTABLE INTERVALS OF ALMO--ETC(U)
JAN 77 E P CERNOCKY, E KREML
RPI-CS-77-1

N00014-76-C-0231

NL

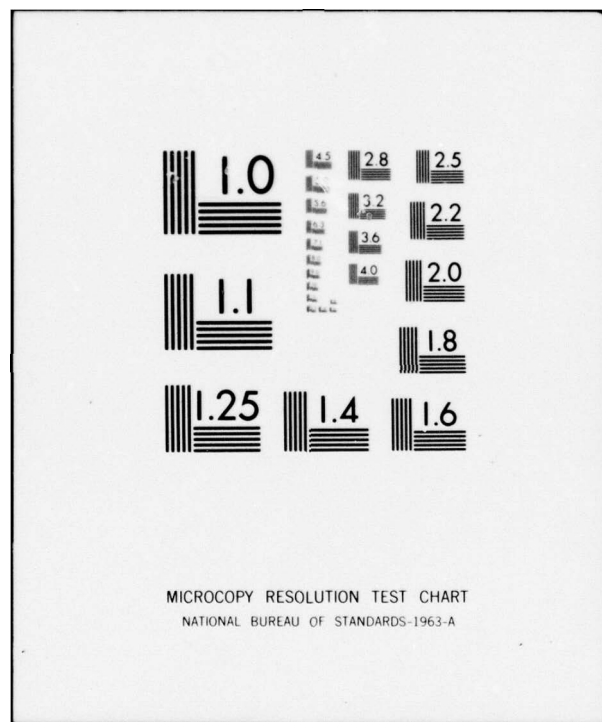
UNCLASSIFIED

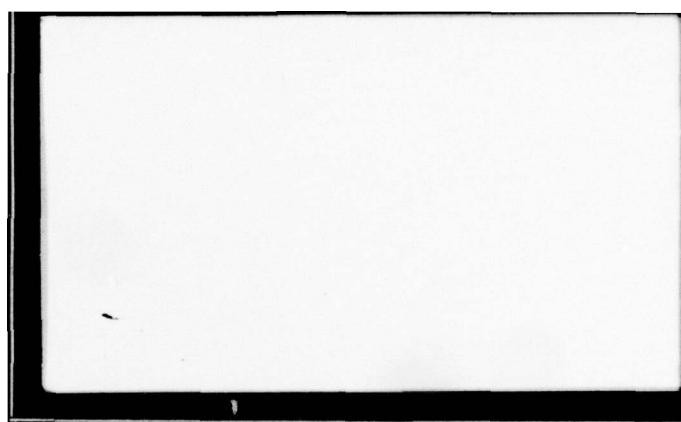
| OF |
AD
A036344
EPC



END

DATE
FILMED
3-77





(12)

NONLINEAR MONOTONIC FUNCTIONS WITH
SELECTABLE INTERVALS OF ALMOST
CONSTANT OR LINEAR BEHAVIOR WITH
APPLICATION TO TOTAL
STRAIN VISCOPLASTICITY

E.P. Cernocky and E. Krempl
Department of Mechanical Engineering,
Aeronautical Engineering & Mechanics
Rensselaer Polytechnic Institute
Troy, New York 12181

Report No. RPI CS 77-1



N00014-76-C-0231

Approved for public release; distribution unlimited.

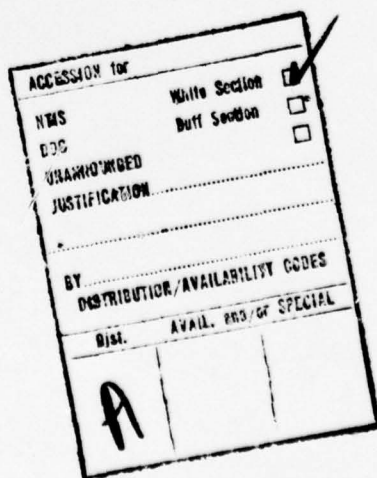
NONLINEAR MONOTONIC FUNCTIONS WITH SELECTABLE INTERVALS OF
ALMOST CONSTANT OR LINEAR BEHAVIOR WITH APPLICATION
TO TOTAL STRAIN VISCOPLASTICITY

E.P. Cernocky and E. Krempel
Department of Mechanical Engineering,
Aeronautical Engineering & Mechanics
Rensselaer Polytechnic Institute
Troy, New York 12181

ABSTRACT

A rather general method is given to construct classes of functions with an arbitrary almost constant (linear) initial interval followed by a non-prescribed interval of monotonic nonlinear behavior. This region of nonlinear behavior is succeeded by an unbounded interval of almost constant (linear) behavior. They contain not more than four selectable parameters and are synthesized from analytic, monotonic, normalized and bounded base functions through the introduction of two separate kernel sets, subsequent addition and integration. As examples we give the special functions based on the error, the hyperbolic tangent, the inverse tangent, a rational and the incomplete gamma function. Limiting function forms, such as the bilinear form, are derived for limiting values of the parameters.

We have found these functions useful in the total strain approach to viscoplasticity, i.e., the analytical modelling of stress-strain diagrams, strain (stress)-rate effects, creep and relaxation curves for monotonic and cyclic loading. Also these functions offer great flexibility in the curve fitting of experimental data generated in the above-mentioned tests.



Introduction

In an attempt to model time (rate)-dependent as well as time (rate)-independent behavior of metals without the use of a yield surface and without the normal decomposition of the small strain tensor into elastic, plastic and creep parts a new total strain approach to inelastic behavior was proposed in [1] after a careful review of the predictive capability of currently used constitutive equations vis a vis experimental evidence [2].

The new approach employs total strain only and recognizes four different phenomena which require different repositories in a constitutive equation.

They are

- nonlinearity
- rate (time)-dependence
- history dependence in the sense of plasticity
- aging.

Rate (time)-independence is obtained as a special case of rate (time)-dependence.

Aging shall be excluded from our considerations in the present paper.

The repository for the modeling of history dependence in the sense of plasticity rests with a microstructure memory function which can discontinuously change at points of unloading [1]. Between successive points of unloading (as defined in [1]) the constitutive equation is a nonlinear elastic and non-linear viscous law for the rate-independent and the rate-dependent case, respectively. The stress and strain tensor at points of unloading are introduced into the constitutive equation to affect initial elastic response upon unloading. The sign of the differential of the second invariant of the stress (strain) tensor measured from the last point of unloading is the loading and unloading criterion [1].

A total strain approach to plasticity or viscoplasticity must be able to reproduce the almost linear behavior of metals for small strains over an almost arbitrary range followed by the strongly nonlinear behavior at the onset of plastic flow. Moreover since the "elastic range" may be changed as a function of prior deformation (cold-working, see Fig.4a in [3]) or of temperature the functions used in a total strain approach must be capable of representing these changes. Our approach requires that this be done by merely changing the constants in the functions used without altering the function form.

An example of such a function is given in [3] for the rate-independent case, whereas the rate-dependent case is treated in [4].

It is the purpose of this paper to give a rather general method of constructing functions of almost constant (linear) behavior over an arbitrary interval followed by nonlinear monotonic behavior over an adjacent interval. Finally, almost constant (linear) behavior is obtained after the region of nonlinearity. We propose a whole family of functions in closed form using not more than four selectable constants. Depending on the value of these constants the value of the function can change within wide limits which make these functions very useful in their application to viscoplasticity.

Construction of Nonlinear, Differentiable Functions with Selectable Intervals of Almost Constant or Linear Behavior

An examination of real stress-strain diagrams and the required properties of functions used in our constitutive theory [1,3,4] indicates the need for the development of a flexible function $Y(X)$ shown together with $Y'(X)$ in Fig.1 which fulfills the following requirements.

The function $Y(X)$ must be odd in X , with $Y'(0) = S_i$; $Y(X)$ must be linear in X over an initial interval $|X| < X_i$, followed by a non-prescribed interval

of monotonic nonlinear behavior. Finally an unbounded interval $|x| > x_f$ follows on which $Y(X)$ must again and thereafter be linear in X with constant slope s_f . We must of course have $x_f > x_i > 0$ and while we are primarily interested in the case $s_i > 0$, $s_f > 0$, we may consider any other finite values of s_i and s_f .

We choose to develop a representation of $Y(X)$ which is a real valued analytic function in X for all finite X^* . We turn to the development of Y -functions which are approximately linear over the selectable intervals $|x| < x_i$ and $|x| > x_f$. The degree of approximation is controlled by a quality factor which can be arbitrarily selected.

We accomplish our synthesis of $Y(X)$ indirectly, by first constructing $Y'(X)$ and then integrating in X to obtain $Y(X)$. We obtain $Y'(X)$ from the sum of a constant plus two functions such that on specified intervals the net contribution due to the two functions is approximately zero, leaving only the constant behavior. For this purpose we now introduce the function $F(X)$; let $F(X)$ satisfy the following requirements:

$F(X)$ must be a real valued analytic function of the real variable X^*

$F(X)$ must be odd in X

$F(X)$ must be bounded at $X = \infty$ and normalized so that $F(\infty) = 1$

$F(X)$ must be monotonic increasing as X increases

$F'(X)$ must be finite, positive, and monotonic decreasing for non-negative X .

The form of $F(X)$ is that shown in Fig.2a. It indicates a property of $F(X)$ which follows from our requirements: For $|x|$ beyond some selected non-negative

* We subsequently consider cases of functions which are differentiable but not analytic at $X = 0$.

value which we will call λ_0 (no relation to the Lamé constant) which is shown in Fig. 2a, we may regard $|F(X)|$ as approximately constant and equal to 1. We may select λ_0 as large as we deem necessary in order to consider $F(X)$ constant for $|x| > \lambda_0$.

We define a quality factor Q by the relation $Q = 1 - F(\lambda_0)$. Then Q is the upper bound of relative error from F being exactly equal to one which we are willing to accept. Exactly constant behavior of $F(X)$, corresponding to perfect quality, would have $Q = 0$; while a total lack of quality, which would regard any deviation of $F(X)$ from unity as negligible and which would enable us to regard any $F(X)$ value on $[0, 1]$ as constant in X and equal to 1, would correspond to $Q = 1.0$ or 100%. Within the scope of our theory we may choose any Q within the range $0 < Q \leq 1$, with $Q = 0$ not an admissible choice. Thus we are free to select the quality of our approximation to constant behavior (constant slope) over a continuous range from total lack of quality to any arbitrary nearly perfect but never exactly perfect quality.

We may select $Q = .5\%$ if we wish to regard $F(X)$ as constant and equal to one when its true magnitude is on the interval $(.995, 1.0]$ and $F(X)$ as nonconstant, varying with X , when its magnitude is less than .995; this choice of $Q = .5\%$ would then correspond to a choice of $\lambda_0 = F^{-1}(1 - Q) = F^{-1}(.995)$.

We see that the choice of Q , with Q restricted to $0 < Q \leq 1$, and the particular function chosen for F determine uniquely the value of λ_0 . Henceforth we will use the term "constant behavior" to mean behavior which is approximately constant to an accuracy commensurate with the value of the factor Q , and we will use the term "linear behavior in X " to denote the behavior of a function which is approximately linear in X , and where the slope of this function is then approximately constant to a degree of accuracy commensurate with the value of the quality factor Q .

Appendix A lists particular $F(X)$ functions which we have used so far.

Kernel Forms

We now introduce two sets of kernel functions of X : the set $U_1(X)$, $V_1(X)$ and the set $U_2(X)$, $V_2(X)$ which enable us to develop two distinct forms of $Y(X)$.

The First Set of Kernel Forms

Define

$$U_1(X) = \lambda_o + 2\lambda_o \left(\frac{x_i + X}{x_f - x_i} \right) \quad (1)$$

and

$$V_1(X) = \lambda_o + 2\lambda_o \left(\frac{x_i - X}{x_f - x_i} \right). \quad (2)$$

Note that $U_1(0) = V_1(0) > 0$ since $x_f > x_i > 0$. Recalling the form of $F(X)$, we have for $F(U_1(X))$ and $F(V_1(X))$ the forms shown respectively in Figs. 3a and 4b. We may interpret $U_1(X)$ as a translation of the vertical axis and a rescaling (stretch) of the horizontal (X)-axis; and we may interpret V_1 as a translation of the vertical axis and a reflection and rescaling (stretch) of the horizontal (X)-axis. We now add the two functions $F(U_1(X))$ plus $F(V_1(X))$ to obtain the form indicated in Fig. 3c. From the required behavior of the F -functions, and as is indicated in Fig. 3c, the sum $(F(U_1) + F(V_1))$ is constant on the interval $|X| < x_i$ and again constant on the unbounded interval $|X| > x_f$ to within an accuracy commensurate with the choice of quality factor Q . It is extremely important to observe that while these two intervals of constant behavior of $F(X)$ must be joined by an interval of nonlinear behavior whose curvature depends upon the particular choice of the function F , the intervals of constant behavior may extend beyond the value of $\pm x_i$ and may commence before $|X|$ attains the value x_f . That is, x_i and x_f absolutely do not denote the points at which $F(X)$ respectively begins and ends nonconstant, nonlinear behavior; rather they specifically denote those $|X|$ points at which $F(X)$ must for $|X|$ values less than x_i or larger than x_f be constant in behavior. The

particular choice of F will determine the size of any excess interval of constant behavior in $|X|$ exceeding x_i or preceding x_f .

We now obtain $Y'(X)$ by multiplying $(F(U_1) + F(V_1))$ by a scale constant A_1 and adding the constant s_f to this sum:

$$Y'(X) = s_f + A_1(F(U_1(X)) + F(V_1(X))) . \quad (3)$$

Since $U_1(0) = V_1(0)$ and since $Y'(0) = s_i$ we have

$$A_1 = \frac{(s_i - s_f)}{2F(U_1(0))} . \quad (4)$$

Clearly $Y'(X)$ is constant over the desired intervals since $Y'(X)$ is constructed from the sum $(F(U_1) + F(V_1))$ which is constant on these intervals.

Let $T(X)$ denote the integral of $F(X)$

$$T(X) = \int^X F(\xi) d\xi .$$

Then from (3) we have

$$Y(X) = s_f X + B_1(T(U_1(X)) - T(V_1(X))) \quad (5)$$

$$B_1 = A_1(x_f - x_i)/(2\lambda_o) \quad (6)$$

with $0 < Q \leq 1$, $\lambda_o = F^{-1}(1-Q)$, and with $x_f > x_i > 0$, s_i , s_f as defined in Fig.1.

Although the parameters x_f , x_i , s_f , s_i may be selected to be material parameters which characterize a given specific material, λ_o is absolutely not a material parameter. The parameter λ_o scales the kernels of the Y' -function to obtain the desired constant behavior, and consequently λ_o is a quality-controlling variable which must be selected. A change in the selection of the F -function used to represent $Y'(X)$ and $Y(X)$, for a fixed chosen quality factor Q , will result in a change in the value of λ_o .

For the special case of some limiting values of the parameters x_i , x_f , s_i , s_f , $Y(X)$ in (5) can yield indeterminate limits. In this case we reconstruct $Y(X)$ from the limiting parameter form of $Y'(X)$ in (3) which is then integrated. The results are given in Appendix B.

The Second Set of Kernel Forms

An alternative, useful set of kernel forms is

$$U_2(X) = -\lambda_o + R(x_f + X) \quad (7)$$

and

$$V_2(X) = -\lambda_o + R(x_f - X) \quad (8)$$

where $R > \lambda_o/x_f$. Here we have completely abandoned utilization of the parameter x_i and have instead elected to introduce a new parameter R , not related to x_i , which we shall refer to as the "amplitude constant" and which is subject to the constraint $R > \lambda_o x_f^*$. Figures 2b and 2c illustrate graphically the forms of $F(U_2(X))$ and $F(V_2(X))$. As in the case of the previous kernel forms, we may regard the kernel U_2 as a translation of the vertical axis and a rescaling (stretch) of the horizontal (X)-axis, and we may regard V_2 as a translation of the vertical axis and a reflection and rescaling (stretch) of the horizontal axis. Again we add two F-function forms to obtain the sum $(F(U_2) + F(V_2))$ which appears graphically in Fig. 2d. Note that in this case, as a result of the use of our new kernel choices, although the resultant function sum is again initially constant on a symmetric interval about the origin, we can no longer discuss or suggest a minimum bound (x_i) upon the size of this interval.

* In Appendix B we consider the limiting case $R \rightarrow \lambda_o/x_f$.

However, since we have retained use of the parameter x_f in our new kernels, and since R is greater than λ_o/x_f , and since $F(X)$ is constant for $|X|$ greater than λ_o , we are able to conclude, exactly as in the case of our previous kernel forms, that the function sum $(F(U_2) + F(V_2))$ is constant for all X on the unbounded intervals $|X| > x_f$. Multiplying the sum $(F(U_2) + F(V_2))$ by a scale constant A_2 and adding the constant s_f enables us to represent $Y'(X)$ in terms of the second set of kernels:

$$Y'(X) = s_f + A_2(F(U_2(X)) + F(V_2(X))) \quad (9)$$

since $Y'(0) = s_i$ and $U_2(0) = V_2(0) > 0$ we have

$$A_2 = \frac{s_i - s_f}{2F(U_2(0))} \quad (10)$$

and integration of (9) in terms of $T(X)$ results in

$$Y(X) = s_f X + B_2(T(U_2(X)) - T(V_2(X))) \quad (11)$$

with

$$B_2 = A_2/R. \quad (12)$$

Clearly $Y(X)$ is linear in X for $|X| > x_f$ because of our synthesis of $Y(X)$ from the function sum $(F(U_2) + F(V_2))$ which is constant on the interval $|X| > x_f$; because of this linearity we will refer to the region $|X| > x_f$ as the region of steady-state behavior of $Y(X)$, or the steady-state region.

Because $Y(X)$ is linear in its steady-state behavior, the effect of varying the selection of the amplitude parameter R is to translate vertically the steady-state Y -curve. Then over the range of admissible R and the limiting R -values, i.e., $\Re[\lambda_o/x_f, \infty]$, for any fixed choice of s_i , s_f , positive x_f , and steady-state X , there is one R -value, denoted as R_{\min} , which renders the smallest possible value of $|Y(X)|$, and there is one R -value, denoted as R_{\max} , which renders the largest possible value of steady-state amplitude $|Y(X)|$. The

values of R_{\min} and R_{\max} are independent of the specific values of S_i and S_f and depend only upon the ranges of S_i and S_f . Examination of the $Y(X)$ -function indicates that for the cases S_i positive and greater than S_f or S_i negative and less than S_f , R_{\min} is finite and $R_{\max} = \infty$; for the converse cases of S_i positive but less than S_f or S_i negative and greater than S_f , R_{\max} is finite and $R_{\min} = \infty$. Consequently, the effect of the choice of S_i , S_f combinations determines whether $R = \infty$ corresponds to R_{\max} or to R_{\min} ; and whether a particular finite critical R -value corresponds to R_{\min} or to R_{\max} .

Throughout this report we will consider the case $S_i > S_f \geq 0$. In this case $R_{\max} = \infty$ and R_{\min} must either be the lower limit of the range of admissible R , equal to λ_o/x_f , or R_{\min} must be an R -value which satisfies the constraint $dY(X; R)/dR = 0$.

Since the numerical value of R_{\min} is independent of the particular values of S_i and S_f while depending upon the ranges of these values, the numerical value of R_{\min} then depends only upon the F -function used, the chosen quality factor, the value of x_f , and the choice of the steady-state X -value. As a consequence of the linear behavior of $Y(X)$ in its steady-state regions, varying the choice of X within the steady-state region will not change the minimizing value of R_{\min} . By considering the limiting case of $X \rightarrow \infty$ we obtain a transcendental relationship enabling us to write and use $R_{\min} = R_{\min}(x_f)$ for any given particular F -function choice and desired quality factor Q . A derivation of the relation $R_{\min}(x_f)$ for a particular function choice appears in Appendix C.

While a decrease of R below the value R_{\min} and on the interval $R_{\min} > R \geq \lambda_o/x_f$, will result in an increase in the steady-state amplitude, this range of amplitude is contained as a subset of the amplitude range corresponding to R increasing beyond R_{\min} . Consequently for X in the steady-state regions and

x_f fixed, increasing R beyond R_{min} allows us to sweep the entire range of available steady-state amplitudes. The parametric dependence of $Y(X)$ upon the amplitude parameter R is illustrated in Figs. 4 and 5. In Fig. 4 the band of available $Y(X)$ -curves for $R_{min} \leq R \leq \infty$ is shown. Figure 5 shows the variation of Y as a function of R and the value of R_{min} is clearly identifiable. It is further evident that $\text{Re}[R_{min}, \infty]$ contains the amplitude values of steady-state $Y(X)$ for $\text{Re}[\lambda_0/x_f, R_{min}]$.

Because of this particular parametric dependence of the $Y(X)$ -function upon R , we now propose to reduce our admissible range of R to $\text{Re}[R_{min}, \infty]$; no other R -values need be considered.

Discussion

Both sets of kernel forms can be used with any of the functions listed in Appendix A. A great variety of $F(X)$ function choices are at our disposal. If necessary, the set of available function choices can be enlarged by adding new functions satisfying the requirements placed upon the form of $F(X)$, and by considering linear combinations of available $F(X)$ forms.

To describe a particular $Y(X)$ four independent parameters must be selected. The initial and final slope, s_i and s_f , respectively are common to both kernel sets. In addition, for the first kernel set x_i and x_f can be prescribed provided $x_f \geq x_i > 0$. In the case of the second kernel form R and x_f can be selected subject to the restriction $\text{Re}[R_{min}, \infty]$ where $R_{min} \geq \lambda_0/x_f$.

Both kernel forms yield linear (B2, B11, B20, B24) or bilinear behavior (B15 and B28) for limiting values of the parameters. These "linear" forms of $Y(X)$ are independent of $F(X)$.

To obtain numerical values of $Y(X)$ calculators must be used. For the hyperbolic tangent, the inverse tangent and the rational function representations

of $F(X)$, $Y'(X)$ and $Y(X)$ can be easily calculated using an "electronic slide-rule". We have found it useful to employ a central computer and illustrate the results by graphs of $Y'(X)$ and $Y(X)$. Some of them are reproduced below to illustrate the properties of the functions.

Figure 6 shows the behavior of the normalized $Y'(X)$ function, Eq. (3), for $F(X)$ based on the error function (A1) and the hyperbolic tangent function (A5), respectively. The constant behavior for $|X|/X_i < 1$ and $|X|/X_i > 3$ for both functions is evident as well as the different behavior in the nonconstant region. (The ratio $\mu = X_f/X_i$ determines the interval of constant behavior. We emphasize that $Q = 0.005$ in both cases.)

The influence of the selection of $\mu = X_f/X_i$ on the behavior of $Y'(X)$ is illustrated in Fig. 7. As μ increases from 1.1 to 3.5 the transition from S_i to S_f becomes more gradual. This graph also shows that although constant behavior is definitely obtained for $|X|/X_i < 1$ and $|X|/X_i > \mu$, it may extend beyond $|X|/X_i = 1$ and commence before $|X|/X_i = \mu$. (The comparison between the $\mu = 1.1$ and the $\mu = 3.5$ curves illustrates this point very well.) Although the transition for $\mu = 1.1$ appears very sharp on the graph, the $Y'(X)$ for $\mu = 1.1$ is analytic. (Note, that a jump discontinuity would be obtained at $|X|/X_i = 1$ for $\mu = 1$, Eq. (B14).)

Figure 8 shows the parametric dependence of $Y'(X)$ on the ratio S_f/S_i illustrating that S_f and S_i may be arbitrarily selected.

The next three graphs are illustrations of the capabilities of the second set of kernel forms for $Y(X)$. In these illustrations $Y(X)$ is identified with Cauchy stress σ and X assumes the role of strain ϵ because of the obvious resemblance of the $Y(X)$ vs X -curves to the stress-strain diagram.

Figure 9 shows σ/S_i vs strain based on Eqs. (11) and (A1) for various values of X_f for fixed S_i and S_f . At each value of X_f , $R = R_{\min}$, so that we have

drawn the lowest possible curve for each x_f -value. Therefore, at each value of x_f higher curves could be obtained by increasing R beyond R_{\min} , see Fig.4.

For $x_f = 0.002$ we have graphed the bilinear limiting form for $R = \infty$ in addition to the curve for R_{\min} . By increasing R beyond R_{\min} , $Y(X)$ -curves higher than the curve for R_{\min} but lower than the curve for $R = \infty$ can be obtained.

In the discussion of the rational function form of $Y(X)$, Eq. (A16), we mentioned that each choice of the exponent ξ determines a different function. This is illustrated in Fig.10 where stress-strain curves for $\xi = 3$ and $\xi = 11$ for the same x_f -values are displayed, respectively. At each x_f , $R = R_{\min}(x_f)$. It is seen that the curves for $\xi = 11$ are higher than those for $\xi = 3$. By coincidence the curve for $x_f = 0.004$ and $\xi = 3$ overlaps almost everywhere with the curve $x_f = 0.001$ and $\xi = 11$. The curve for $x_f = 0.001$ and $R = \infty$ is drawn for comparison. This limiting curve applies to both values of the exponent ξ . The flexibility of the rational function is obvious.

Finally Fig.11 uses a different scale for the strain and a negative value for s_f and illustrates that this choice is also possible for $Y(X)$ based on Eq. (11).

Application

From the discussion of Figs.9 - 11 it is obvious that the $Y(X)$ -functions developed from the second set of kernel forms are most suitable for approximating experimentally determined stress-strain diagrams. The slopes s_i , s_f as well as the value of x_f are immediately obtained from these diagrams. For each $F(X)$ -function R_{\min} can be calculated by the procedure given in Appendix C. The resulting minimum $Y(X)$ -curve can be computed and compared with the diagram to be matched. If the diagram is above $Y(X)$ for $R = R_{\min}$, the R that results

in the best approximation can be found. If the diagram is below $Y(X)$ for $R = R_{\min}$, another function $F(X)$ must be chosen and the procedure repeated.

We recall that the use of the second set of kernel forms does not permit an easy identification of the extent of the linear behavior of $Y(X)$ in the vicinity of $X = 0$. It would therefore appear that the first kernel form would offer advantages if an initial interval of almost linear behavior is of interest. However, the choice of the first kernel set permits the specification of this interval but does not allow us to control the amplitude of the steady-state $Y(X)$ -curve. It is for this reason that the second set of kernel forms is preferred for application to stress-strain diagrams.

Another application of the $Y'(X)$ and $Y(X)$ -functions is in the identification of coefficient functions of nonlinear constitutive laws such as the differential form proposed in [4], Eq. (3). The $Y(X)$ -function is then identified with $g(\epsilon)$ and the $Y'(X)$ -function assumes the role of $m(\sigma)$. This function is responsible for modeling the nonlinear stress dependence of the creep rate which is observed in metals, see Eq. (9) in [4]. It is shown in [4] that "numerical experiments" using the same functions but different values of parameters can change the "character" of the results. As a specific example, $S_f = 0$ in the $Y(X)$ used for $g(\epsilon)$ reproduces secondary creep whereas $S_f > 0$ produces primary creep only; see Eq. (10) and Figs. 7 and 8 in [4].

Also the almost linear-elastic, rate-independent initial range found in stress-strain diagrams obtained at various strain rates can be reproduced with the differential form, Eq. (3) in [4] if $g(\epsilon)$ has the initial almost linear region of $Y(X)$ and $m(\sigma)$ and $k(\epsilon)$ are almost constant as is the case for the $Y'(X)$ -functions; see Figs. 1 and 2 in [4].

A further potential application is in the modeling of history dependence in the sense of plasticity. By making x_f and R depend upon prior deformation

history, which is possible through the structure memory function [1,3], the graphs in Fig.9 could be interpreted as stress-strain diagrams after various amounts of prior cold work.

The parameters in $Y(X)$ can also be considered to be dependent on temperature and the graphs in Fig.9 can be interpreted as having been obtained at various temperatures. Although S_i and S_f are kept constant in Fig.9, they can be changed to any desired value if such a need arises in application.

Basically the functions developed herein serve the same purpose as the one proposed in [3]. Also they permit the application to rate-dependence (viscoplasticity). Their closed form makes them comparatively easy to use.

Acknowledgement

The sponsorship of the Office of Naval Research and of the National Science Foundation is gratefully acknowledged. During part of this work the second author was DFG-Richard-Merton Visiting Professor at the Institut für Statik und Dynamik der Luft- und Raumfahrtkonstruktionen Universität Stuttgart. The partial support of the Deutsche Forschungsgemeinschaft during the sabbatical is acknowledged.

REFERENCES

1. Krempl, E., On the Interaction of Rate and History Dependence in Structural Metals, *Acta Mechanica* 22, 53-90 (1975).
2. Krempl, E., Cyclic Creep - An Interpretive Literature Survey, *Welding Research Council Bulletin No.195*, 1974.
3. Liu, M.C.M., E. Krempl and D.C. Nairn, An Exponential Stress-Strain Law for Cyclic Plasticity, *Trans. ASME, J. of Eng. Materials and Technology*, 98, 322-329 (1976).
4. Krempl, E., E.P. Cernocky and M.C.M. Liu, The Representation of Visco-plastic Phenomena in Constitutive Equations, pp.95-114 in "Constitutive Equations in Viscoplasticity. Computational and Engineering Aspects," J.A. Stricklin and K.J. Saczalski editors, AMD Vol.20, ASME, New York, NY 1976.
5. Handbook of Mathematical Functions, Ed. by Milton Abramowitz and Irene Stegun, Dover Publications, Inc., New York, published in 1965, 8th printing, p.260, Eq.6.5.2.

FIGURE CAPTIONS

- Figure 1** Schematic representation of the function $Y(X)$ and its derivative $Y'(X)$ (stress-strain diagram). For $|X| < X_i$ and for $|X| > X_f$ almost linear (constant) behavior is observed.
- Figure 2** Schematic illustration of $F(X)$, Fig. 2a; the axes are translated stretched (Fig. 2b); translated, reflected and stretched (Fig. 2c). The addition of $F(U_2)$ and $F(V_2)$ yields within a constant the desired $Y'(X)$ -form, Fig. 2d.
- Figure 3** The axes are translated and stretched by U_1 (3a) and translated, reflected and stretched by V_1 (3b) before $F(U_1)$ and $F(V_1)$ are added (3c). Figure 3c represents (within a constant) the desired $Y'(X)$ -form.
- Figure 4** Schematic showing the dependence of $Y(X)$ on the parameter R for $R_{\min} \leq R \leq \infty$. Note that for $R = \infty$ bilinear behavior is obtained. The other parameters S_i , S_f and X_f are held constant.
- Figure 5** The dependence of Y on the parameter R for $X = .003$ at three different values of X_f . The curves are based on $F(X) = ERF(X)$ and exhibit the minimizing value of R . In our application we restrict R to $R > \lambda_o/X_f$.
- Figure 6** The normalized function $Y'(X)$, Eq. (3), based on the error function Y'_{erf} , Eq. (A3), and on the hyperbolic tangent function Y'_{tanh} , Eq. (A7); $\mu = X_f/X_i = 3$, $S_f/S_i = .25$, $Q = 0.005$ in both cases.
- Figure 7** The influence of the choice of $\mu = X_f/X_i$ on $Y'(X)$. $Y'(X)$ is based on Eqs. (3), (A3) and $S_f/S_i = .25$, $Q = 0.005$.
- Figure 8** $Y'(X)$ at different values of S_f/S_i with constant $\mu = X_f/X_i = 3$. $Y'(X)$ is based on the error function, Eqs. (A3) and (3), $Q = 0.005$.
- Figure 9** σ/S_i -curves based on Eqs. (11) and (A4). At each X_f , $R = R_{\min}(X_f)$. For $X_f = 0.002$ the bilinear form ($R = \infty$) is also shown.
 $\sigma \equiv Y(X)$; $X \equiv \epsilon$ (strain); $S_i = 21.7 \times 10^6$ psi (≈ 150 GPa),
 $S_f/S_i = 0.02$, $Q = 0.005$.

Figure 10 σ/S_i -curves based on Eqs. (11) and (A16) for $\xi = 3$ and $\xi = 11$ at various X_f . For each X_f , $R = R_{\min}(X_f)$. For $X_f = .001$ the bilinear form ($R = \infty$) is also shown. $S_i = 21.7 \times 10^6$ psi (≈ 150 GPa), $S_f/S_i = 0.02$, $Q = 0.005$.

Figure 11 σ/S_i -curves based on Eqs. (11) and (A4) for negative S -values and expanded scale. $R = R_{\min}(X_f)$. For $X_f = 0.01$ the bilinear form ($R = \infty$) is also drawn in. $S_i = 21.7 \times 10^6$ psi (≈ 150 GPa), $S_f/S_i = -0.005$, $Q = 0.005$.

APPENDIX A

PARTICULAR CHOICES FOR THE $F(X)$, $T(X)$, $Y'(X)$ AND $Y(X)$ FUNCTIONS

For convenience we will be using generalized kernels U , V and constants A , B . Then if use of the first kernel set is desired, the set U , V , A , B are to assume the values of the set U_1 , V_1 , A_1 , B_1 as defined in Eqs. (1), (2), (4), (6). For the second kernel set U , V , A , B will assume the values given in Eqs. (7), (8), (10), (12).

1) Error Function

$$F(X) = \operatorname{erf}(X) \quad \text{with} \quad \operatorname{erf}(\infty) = 1 \quad (\text{A1})$$

$$T(X) = X \operatorname{erf}(X) + \frac{1}{\sqrt{\pi}} \exp(-X^2) \quad (\text{A2})$$

$$Y'(X) = S_f + A(\operatorname{erf}(U) + \operatorname{erf}(V)) \quad (\text{A3})$$

$$Y(X) = S_f X + B(U \operatorname{erf}(U) - V \operatorname{erf}(V) + \frac{1}{\sqrt{\pi}} (\exp(-U^2) - \exp(-V^2))) \quad (\text{A4})$$

2) Hyperbolic Tangent Function

$$F(x) = \tanh(x) \quad (\text{A5})$$

$$T(X) = \ln(\cosh(X)) \quad (\ln \text{ is base e}) \quad (\text{A6})$$

$$Y'(X) = S_f + A(\tanh(U) + \tanh(V)) \quad (\text{A7})$$

$$Y(X) = S_f X + B \ln\left(\frac{\cosh(U)}{\cosh(V)}\right) \quad (\text{A8})$$

3) Inverse Tangent Function

$$F(X) = \frac{2}{\pi} \arctan(X) \quad (\text{A9})$$

$$T(X) = \frac{2X}{\pi} \arctan(X) - \frac{1}{\pi} \ln(1+X^2) \quad (\text{A10})$$

$$Y'(X) = S_f + \frac{2A}{\pi} (\arctan(U) + \arctan(V)) \quad (\text{A11})$$

$$Y(X) = S_f X + \frac{2B}{\pi} \left(U \arctan(U) - V \arctan(V) - \frac{1}{2} \ln\left(\frac{1+U^2}{1+V^2}\right) \right) \quad (\text{A12})$$

4) Rational Function*

$$F(x) = \text{sign}(x) \left(1 - \left(1 + |x| \right)^{1-\xi} \right), \quad \xi > 2 \quad (\text{A13})$$

$$T(x) = |x| + \frac{1}{(\xi-2)} (1 + |x|)^{2-\xi} \quad (\text{A14})$$

$$Y'(x) = S_f + A [\text{sign}(U) (1 - (1 + |U|)^{1-\xi}) + \text{sign}(V) (1 - (1 + |V|)^{1-\xi})] \quad (\text{A15})$$

$$Y(x) = S_f x + \frac{B}{(\xi-2)} [(\xi - 2) (|U| - |V|) + (1 + |U|)^{2-\xi} - (1 + |V|)^{2-\xi}] \quad (\text{A16})$$

5) Incomplete Gamma Function*

$$F(x) = \text{sign}(x) \gamma\left(\frac{1}{\omega}, |x|^{\omega}\right) / \Gamma\left(\frac{1}{\omega}\right), \quad \omega > 0 \quad (\text{A17})$$

$$T(x) = \frac{1}{\Gamma\left(\frac{1}{\omega}\right)} \left[|x| \gamma\left(\frac{1}{\omega}, |x|^{\omega}\right) - \gamma\left(\frac{2}{\omega}, |x|^{\omega}\right) \right] \quad (\text{A18})$$

$$Y'(x) = S_f + \frac{A}{\Gamma\left(\frac{1}{\omega}\right)} \left[\text{sign}(U) \gamma\left(\frac{1}{\omega}, |U|^{\omega}\right) + \text{sign}(V) \gamma\left(\frac{1}{\omega}, |V|^{\omega}\right) \right] \quad (\text{A19})$$

$$Y(x) = S_f x + \frac{B}{\Gamma\left(\frac{1}{\omega}\right)} \left[|U| \gamma\left(\frac{1}{\omega}, |U|^{\omega}\right) - |V| \gamma\left(\frac{1}{\omega}, |V|^{\omega}\right) - \gamma\left(\frac{2}{\omega}, |U|^{\omega}\right) + \gamma\left(\frac{2}{\omega}, |V|^{\omega}\right) \right] \quad (\text{A20})$$

where γ is the incomplete gamma function [5] and $\text{sign}(X)$ is defined as

$$\text{sign}(x) = \begin{cases} 1 & x > 0 \\ 0 & x = 0 \\ -1 & x < 0 \end{cases}$$

* Here we introduce $F(x)$ -functions which are not analytic but are differentiable at $x = 0$.

For both the rational and incomplete gamma function each value of ξ and ω , respectively, represent one possible $Y(X)$ -form. Therefore an infinite class of functions with different nonlinear behavior is available.

APPENDIX B

$Y'(X)$ and $Y(X)$ FUNCTION REPRESENTATIONS FOR LIMITING VALUES OF THE PARAMETERS

In some cases the limiting parameter values result in indeterminate forms of $Y(X)$ when Eqs. (5) or (11) are used to represent $Y(X)$. This is a consequence of the construction of $Y(X)$ in (5) or (11) from $Y'(X)$ in (3) or (9) for nonlimiting parameter values. Consequently, when these indeterminate limits arise, we reformulate $Y(X)$ as the integral of the limiting parameter form of $Y'(X)$ in (3) or (9); this procedure is fundamentally consistent with our construction of $Y(X)$ from $Y'(X)$. Alternatively the indeterminate limiting form of $Y(X)$ may be resolved when specific forms of $Y(X)$ are chosen; and in some, but not all cases, general forms of $Y(X)$ can be used for the resolution of the indeterminate limits.

Both sets of kernel forms.

Limit $s_f \rightarrow s_i$.

From Eqs. (3), (4), (5), (6) and (9), (10), (11), (12), we obtain

$$\lim_{s_f \rightarrow s_i} Y'(X) = s_i \quad (B1)$$

$$\lim_{s_f \rightarrow s_i} Y(X) = s_i X \quad (B2)$$

First set of kernel forms.

Limit $x_i \rightarrow 0$.

From (1), (2), (4), (6), the following limits are easily derived

$$\lim_{x_i \rightarrow 0} u_1(x) = \lambda_o + 2\lambda_o x/x_f \quad (B3)$$

$$\lim_{x_i \rightarrow 0} v_1(x) = \lambda_o - 2\lambda_o x/x_f \quad (B4)$$

$$\lim_{X_i \rightarrow 0} A_1 = \frac{s_i - s_f}{2F(\lambda_o)} \quad (B5)$$

$$\lim_{X_i \rightarrow 0} B_1 = \frac{x_f(s_i - s_f)}{4\lambda_o F(\lambda_o)} . \quad (B6)$$

Then $Y'(X)$ and $Y(X)$ are of the forms appearing in (3) and (5), respectively, where the above limiting kernel functions and parameter values are used.

Limit $X_f \rightarrow \infty$

The following limits result:

$$\lim_{X_f \rightarrow \infty} U_1(X) = \lambda_o \quad (B7)$$

$$\lim_{X_f \rightarrow \infty} V_1(X) = \lambda_o \quad (B8)$$

$$\lim_{X_f \rightarrow \infty} A_1 = \frac{s_i - s_f}{2F(\lambda_o)} \quad (B9)$$

Consequently, we have

$$\lim_{X_f \rightarrow \infty} Y'(X) = s_i . \quad (B10)$$

Proceeding consistent with our construction of $Y(X)$ as the integral of $Y'(X)$, we integrate (B10) and obtain

$$\lim_{X_f \rightarrow \infty} Y(X) = s_i X . \quad (B11)$$

Limit $X_i \rightarrow X_f$

For finite positive X_f we have

$$\begin{aligned}
 & \text{for } x > x_f \quad \lim_{x_i \rightarrow x_f} U_1(x) = +\infty ; \quad \lim_{x_i \rightarrow x_f} V_1(x) = -\infty \\
 & \text{for } |x| < x_f \quad \lim_{x_i \rightarrow x_f} U_1(x) = +\infty ; \quad \lim_{x_i \rightarrow x_f} V_1(x) = +\infty \quad (B12) \\
 & \text{for } x < -x_f \quad \lim_{x_i \rightarrow x_f} U_1(x) = -\infty ; \quad \lim_{x_i \rightarrow x_f} V_1(x) = +\infty
 \end{aligned}$$

and

$$\lim_{x_i \rightarrow x_f} A_1 = (s_i - s_f)/2 \quad (B13)$$

Proceeding as before, we obtain first

$$\lim_{x_i \rightarrow x_f} Y^*(x) = \begin{cases} s_i & |x| < x_f \\ s_f & |x| > x_f \end{cases} \quad (B14)$$

and integrate to obtain

$$\lim_{x_i \rightarrow x_f} Y(x) = \begin{cases} \frac{s_i x_f + s_f (x - x_f)}{x_f} & x \geq x_f \\ s_i x & |x| \leq x_f \\ -\frac{s_i x_f + s_f (x + x_f)}{x_f} & x \leq -x_f \end{cases} . \quad (B15)$$

It is significant to note that bilinear behavior is obtained in the limit $x_i \rightarrow x_f$ independent of both the particular $F(x)$ -function and the quality factor Q .

Second set of kernel forms

Limit $x_f \rightarrow \infty$.

From Eqs. (7), (8), (9), (10), (11) we obtain

$$\lim_{x_f \rightarrow \infty} U_2(x) = +\infty \quad (B16)$$

$$\lim_{x_f \rightarrow \infty} V_2(x) = +\infty \quad (B17)$$

$$\lim_{X_f \rightarrow \infty} A_2 = (s_i - s_f)/2 \quad (B18)$$

$$\lim_{X_f \rightarrow \infty} Y'(X) = s_i \quad (B19)$$

$$\lim_{X_f \rightarrow \infty} Y(X) = s_i X. \quad (B20)$$

We note then that for each set of kernels, as $X_f \rightarrow \infty$ $Y(X)$ approaches a function exactly linear for all X , with slope s_i .

Limit $X_f \rightarrow 0$.

For the second kernel set, when $X_f \rightarrow 0$, we must recall the restriction $R > \lambda_o/X_f$; that is, while $X_f \rightarrow 0$ the product RX_f attains a finite value greater than the constant λ_o . Consequently R must approach infinity as X_f approaches zero. Then we have

$$\begin{aligned} \text{for } X > 0 \quad & \lim_{\substack{X_f \rightarrow 0 \\ R \rightarrow \infty}} U_2(X) = +\infty; \quad \lim_{\substack{X_f \rightarrow 0 \\ R \rightarrow \infty}} V_2(X) = -\infty \\ \text{for } X < 0 \quad & \lim_{\substack{X_f \rightarrow 0 \\ R \rightarrow \infty}} U_2(X) = -\infty; \quad \lim_{\substack{X_f \rightarrow 0 \\ R \rightarrow \infty}} V_2(X) = +\infty \end{aligned} \quad (B21)$$

$$\lim_{\substack{X_f \rightarrow 0 \\ R \rightarrow \infty}} A_2 = \text{a positive constant}^*. \quad (B22)$$

* Because of the limits involved, the particular value of this constant will not enter into Y' or Y . Further, note that A_2 is fundamentally defined using $U_2(0)$ and consequently in performing the limit of A_2 we must use $\lim_{\substack{X_f \rightarrow 0 \\ R \rightarrow \infty}} U_2(0)$ rather than using limits on $U_2(X)$ and $V_2(X)$ and then letting $X \rightarrow 0$.

Consequently,

$$\lim_{\substack{X_f \rightarrow 0 \\ R \rightarrow \infty}} Y'(X) = S_f \quad (B23)$$

and

$$\lim_{\substack{X_f \rightarrow 0 \\ R \rightarrow \infty}} Y(X) = S_f X \quad (B24)$$

Limit $R \rightarrow \infty$, X_f finite, positive

We have

$$\text{for } X > X_f \quad \lim_{R \rightarrow \infty} U_2(X) = +\infty ; \quad \lim_{R \rightarrow \infty} V_2(X) = -\infty$$

$$\text{for } |X| < X_f \quad \lim_{R \rightarrow \infty} U_2(X) = +\infty ; \quad \lim_{R \rightarrow \infty} V_2(X) = +\infty \quad (B25)$$

$$\text{for } X < -X_f \quad \lim_{R \rightarrow \infty} U_2(X) = -\infty ; \quad \lim_{R \rightarrow \infty} V_2(X) = +\infty$$

and

$$\lim_{R \rightarrow \infty} A_2 = (S_i - S_f)/2 . \quad (B26)$$

Therefore

$$\lim_{R \rightarrow \infty} Y'(X) = \begin{cases} S_i & |X| < X_f \\ S_f & |X| > X_f \end{cases} \quad (B27)$$

and

$$\lim_{R \rightarrow \infty} Y(X) = \begin{cases} S_i X_f + S_f (X - X_f) & X \geq X_f \\ S_i X & |X| \leq X_f \\ -S_i X_f + S_f (X + X_f) & X \leq -X_f \end{cases} \quad (B28)$$

We note then that taking the limit as R approaches infinity, results in a bilinear form for the $Y(X)$ -function and $Y'(X)$ is discontinuous at $X = X_f$.

The maximum amplitude $|Y(X)|$ at any steady state range of $|X|$, for fixed X_f ,

is then $s_f|x| + x_f(s_i - s_f)$ corresponding to the steady-state amplitude of the bilinear $R = \infty$ response*.

This bilinear $Y(X)$ response for the U_2, V_2 kernel representation and the limit $R = \infty$ is identical to the bilinear $Y(X)$ response which results when the U_1, V_1 kernel set is used with the limit $x_i \rightarrow x_f$.

Limit $R \rightarrow \lambda_o/x_f$, x_f finite, positive

$$\lim_{R \rightarrow \lambda_o/x_f} U_2(x) = \lambda_o x/x_f \quad (B29)$$

$$\lim_{R \rightarrow \lambda_o/x_f} V_2(x) = -\lambda_o x/x_f \quad (B30)$$

$$\lim_{R \rightarrow \lambda_o/x_f} A_2 = \infty \quad (B31)$$

$$\lim_{R \rightarrow \lambda_o/x_f} (F(U_2) + F(V_2)) = 0 \quad (B32)$$

In this limit both our Y' and Y -forms in (9) and (11) are indeterminate.

Resolving this limit we have

$$\lim_{R \rightarrow \lambda_o/x_f} Y'(X) = s_f + (s_i - s_f) \frac{F'(\lambda_o x/x_f)}{F'(0)} \quad (B33)$$

$$\lim_{R \rightarrow \lambda_o/x_f} Y(X) = s_f x + (s_i - s_f) \frac{x_f F(\lambda_o x/x_f)}{\lambda_o F'(0)} \quad (B34)$$

* For $s_i > s_f \geq 0$.

APPENDIX C

DEVELOPMENT OF THE REPRESENTATION $R_{\min}(X_f)$

Herein we will construct the representation of the X_f -dependence of R_{\min} for the case when R_{\min} is finite and $R_{\max} = \infty$. We recall that in the complementary case of either $S_f > S_i \geq 0$ or $S_f < S_i \leq 0$, the values of R_{\min} and R_{\max} reverse so that $R_{\min} = \infty$ and R_{\max} is the finite R-critical point. Note that R_{\min} denotes the R-value that minimizes the steady-state amplitude of $Y(X)$ and R_{\max} denotes the corresponding maximizing value of R.

Proceeding, we regard Y as a function of R, write $Y(X;R)$ and restrict X to $|X| > X_f$; then for $R > \lambda_o/X_f$, Y is an analytic function of R^* . To determine R_{\min} we seek a finite $R > \lambda_o/X_f$ which is a solution to

$$\frac{dY}{dR}(X;R) = 0 \quad (C1)$$

and which satisfies

$$\frac{d^2Y}{dR^2}(X;R) > 0. \quad (C2)$$

From Eq. (C1) and Eqs. (7) - (12) we have, for $R > \lambda_o/X_f$

$$F(U_2)(X_f + X) - F(V_2)(X_f - X) - (1/R)(T(U_2) - T(V_2))(1 + RX_f F'(RX_f - \lambda_o)/F(RX_f - \lambda_o)) = 0. \quad (C3)$$

A similar equation results for the representation of Eq. (C2).

We recall that because $Y(X)$ is linear in X in the steady state X-region, R_{\min} is independent of our particular choice of steady-state X.

Then to greatly simplify the relation (C3) and the representation of (C2),

* This is the case for all functions proposed in Appendix A.

we perform the limit of these relations for $X \rightarrow \infty$ and introduce the parameters β and β_o defined as

$$\beta = RX_f - \lambda_o \geq 0 \quad (C4)$$

$$\beta_o = R_{\min} X_f - \lambda_o \geq 0. \quad (C5)$$

We note that when $R = R_{\min}$, β becomes β_o . The case $\beta = 0$ corresponds to the lower limit of admissible R , $R = \lambda_o/X_f$.

We then get from (C3)

$$\beta(\beta + \lambda_o)F'(\beta) - \lambda_o F(\beta) = 0 \quad (C6)$$

and from the representation of (C2)

$$- (2F'(\beta) + (\beta + \lambda_o)F''(\beta)) > 0. \quad (C7)$$

If Eq. (C6) possesses no positive beta-solution, then R_{\min} corresponds to the lower limit of its admissible range, and hence we have $\beta_o = 0$. If a unique positive β -solution to Eq. (C6) exists, then this is the beta value which determines R_{\min} , and consequently β_o is the unique solution*. If Eq. (C6) possesses multiple solutions they must be substituted into Eq. (C7) and the beta values which do not violate (C7) form a set of admissible beta solutions. To this solution set we must add the lower limiting value $\beta = 0$. We then evaluate $Y(X; R)$ for each of the beta values of this modified solution set. The beta value which results in the smallest Y -value is β_o .

* These two cases apply for the particular $F(X)$ functions presented in Appendix A.

For the Y-value comparison test, it is sufficient to consider any value of $x > x_f$ and any s_f which satisfies $s_i > s_f \geq 0$. By choosing $s_f = 0$ and considering the limiting value $x \rightarrow \infty$, the comparison process is greatly simplified. Substituting beta into $Y(\infty, R)$ and dividing by $s_i x_f$ yields the following function of beta for the comparison test

$$\varphi(\beta) = \lambda_o / ((\beta + \lambda_o)^2 F'(\beta)) = Y(\infty, \frac{\beta + \lambda_o}{x_f}) / s_i x_f . \quad (C8)$$

When multiple solutions to Eq. (C6) exist, we proceed by calculating φ for the beta values of the modified solution set. The beta which results in the smallest value of φ is β_o .

Once we have obtained the value of β_o , Eq. (C5) allows us to determine R_{min}

$$R_{min} = (\beta_o + \lambda_o) / x_f . \quad (C9)$$

Equations (C6) and (C7) show a parametric dependence on λ_o . Should we decide on a different quality factor Q and hence λ_o , we must repeat the process to obtain R_{min} related to this new λ_o .

Next we consider for illustration the $Y(X)$ function relation which result from the hyperbolic tangent function for $F(X)$; hence

$$F(\beta) = \tanh(\beta) \quad (C10)$$

and (C6) becomes

$$\beta(\beta + \lambda_o) \operatorname{sech}^2(\beta) - \lambda_o \tanh(\beta) = 0 . \quad (C11)$$

We now select $Q = .005$ and $\lambda_o = 3$ so that

$$2\beta(\beta + 3) - 3 \sinh(2\beta) = 0 . \quad (C12)$$

The unique solution is $\beta = .4777$ and consequently

$$R_{min} = 3.4777/x_f ; \lambda_o = 3 . \quad (C13)$$

If we instead change the quality so that $Q = .0009$, then $\lambda_o = 3.853$ and Eq. (C11) has the unique solution $\beta = .3783$; then

$$R_{\min} = 4.2313/X_f; \lambda_o = 3.853. \quad (C14)$$

We see from Eq. (C11) that for all admissible λ_o , we always have a unique positive β_o . This is similarly the case when $F(X)$ is the error function.

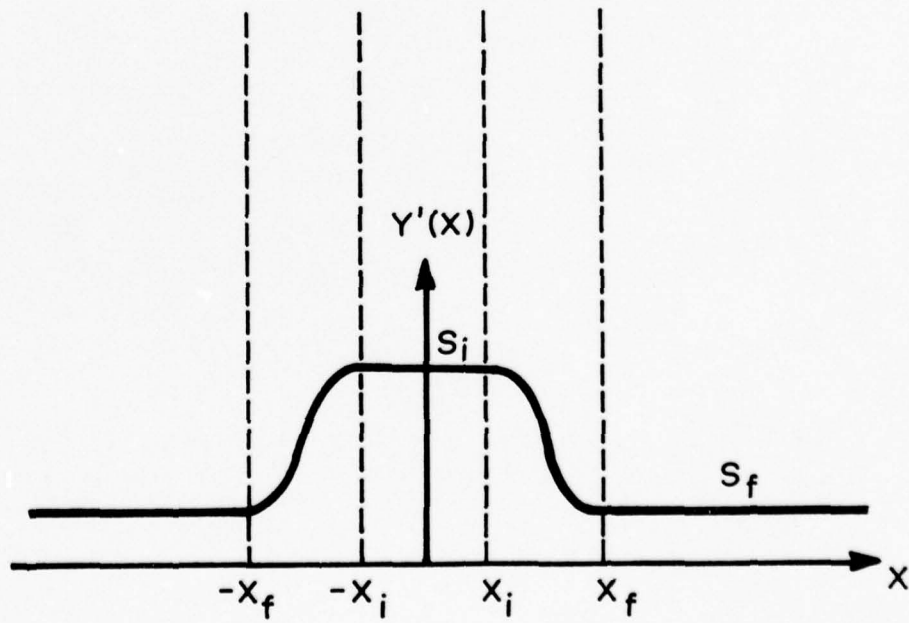
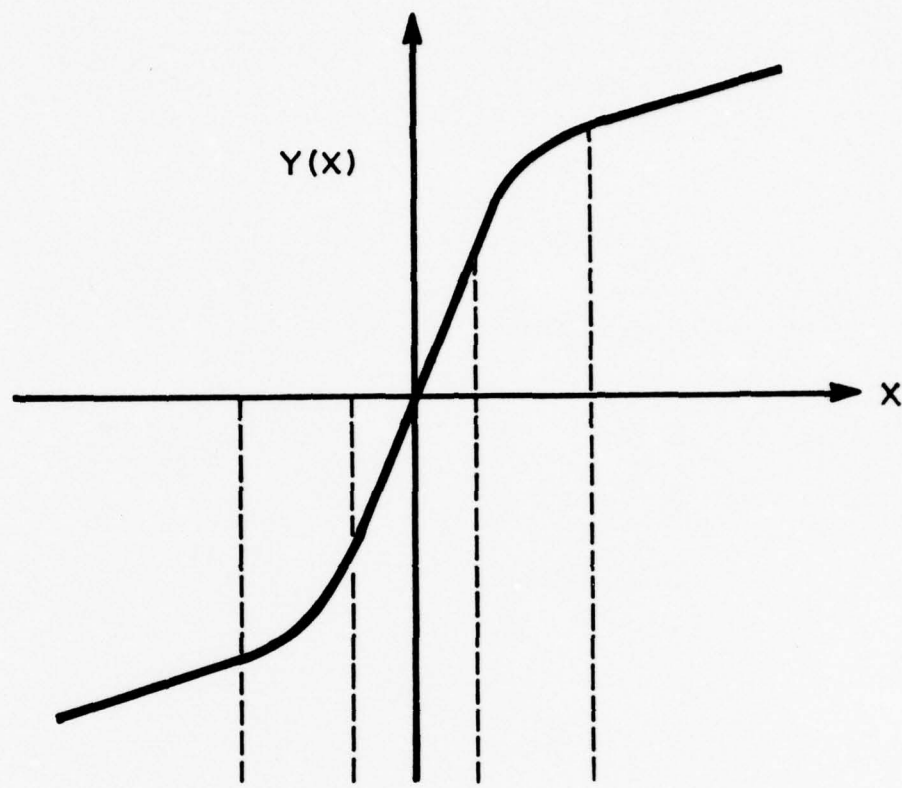


Fig.1

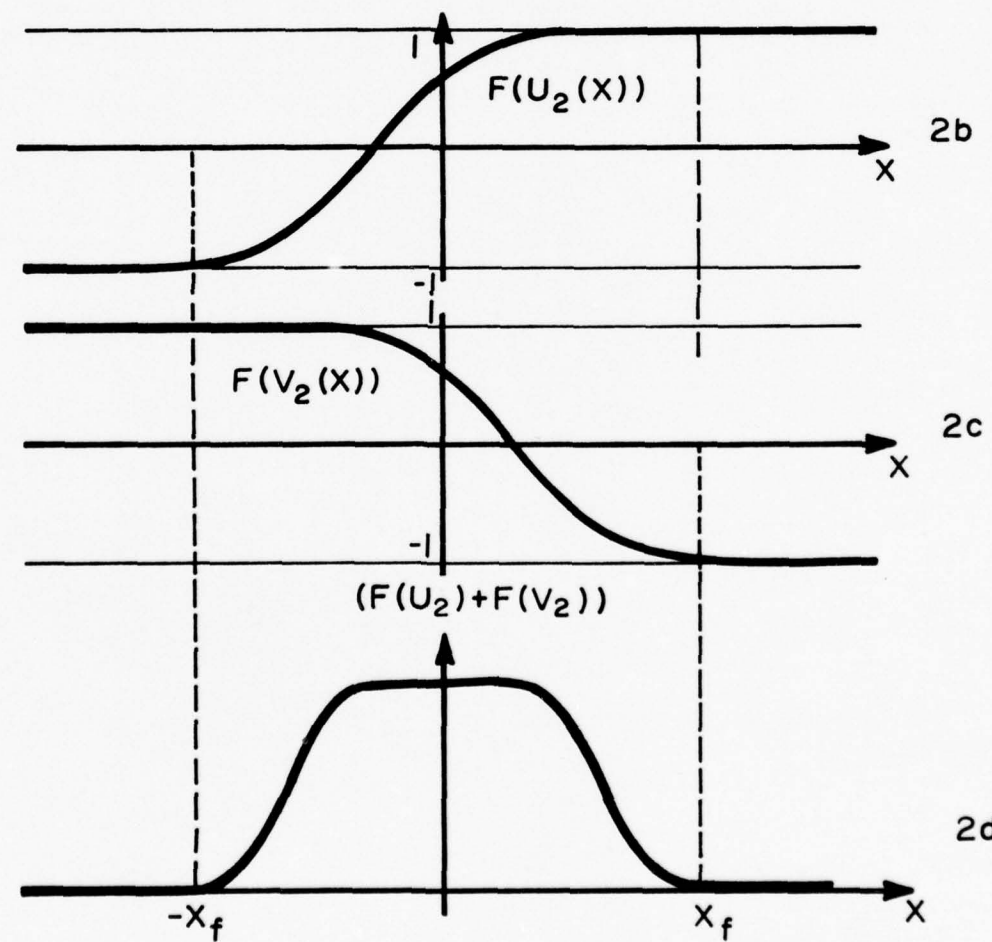
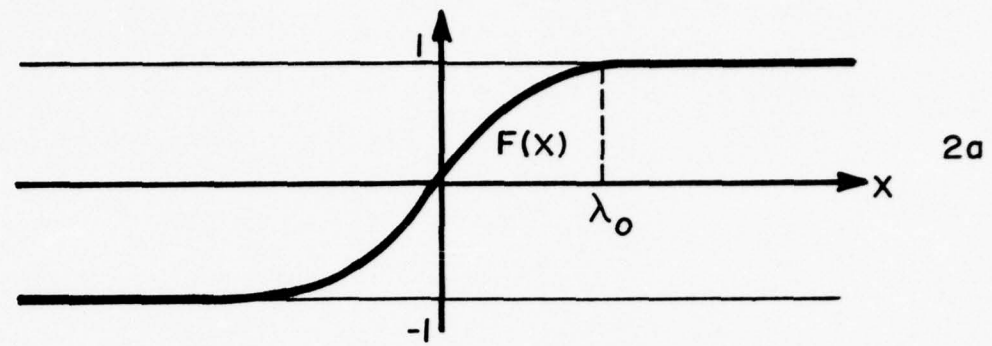


Fig. 2

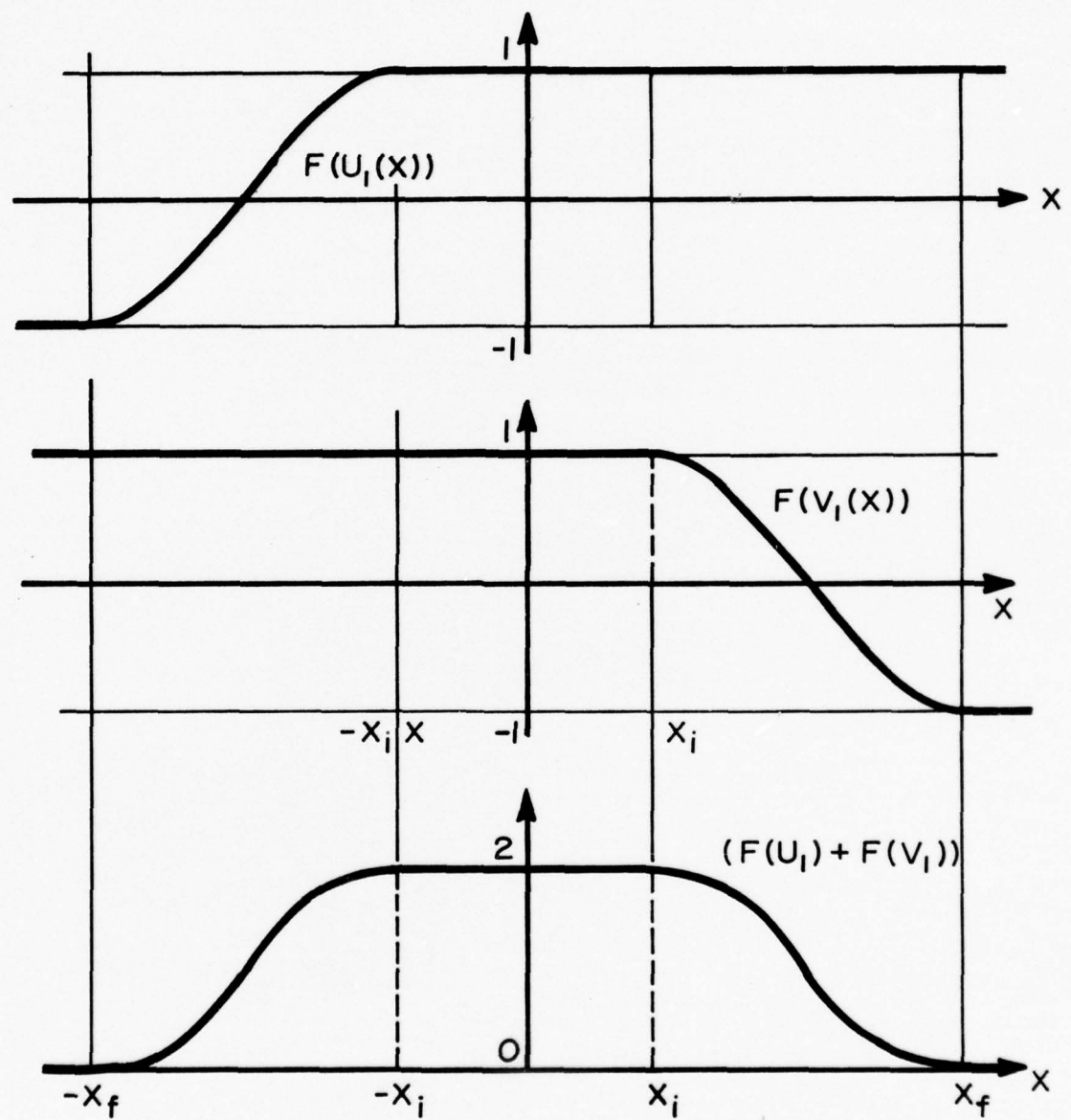
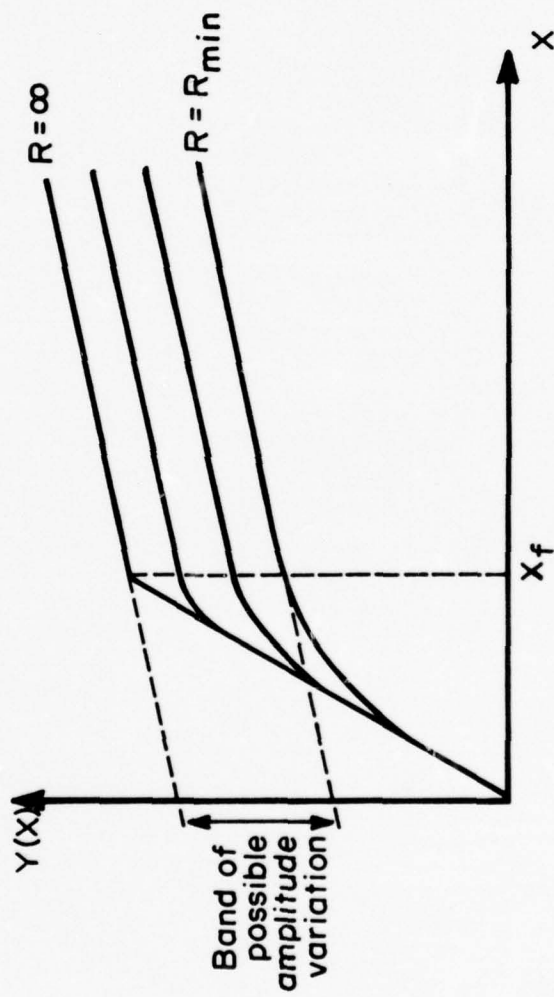


Fig. 3

Fig. 4



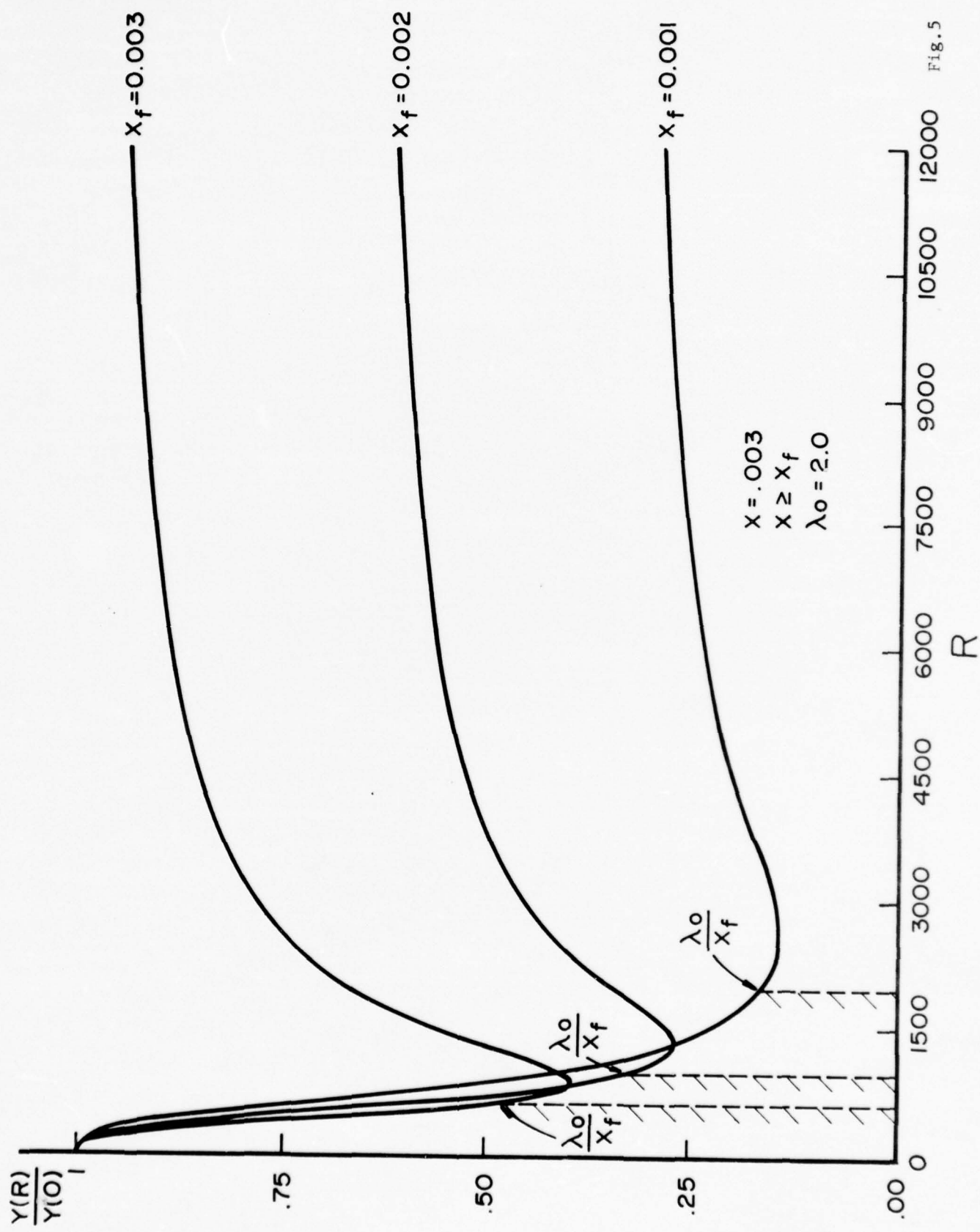
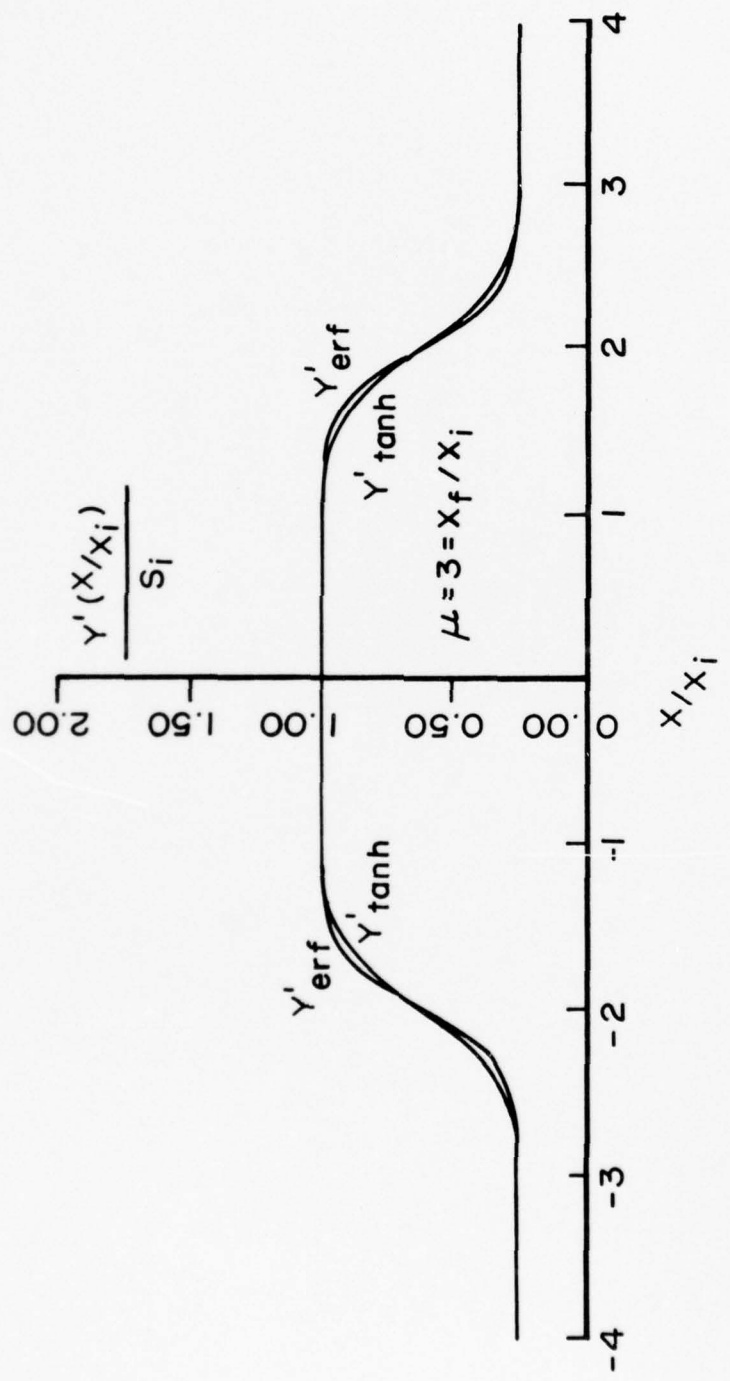


Fig. 6



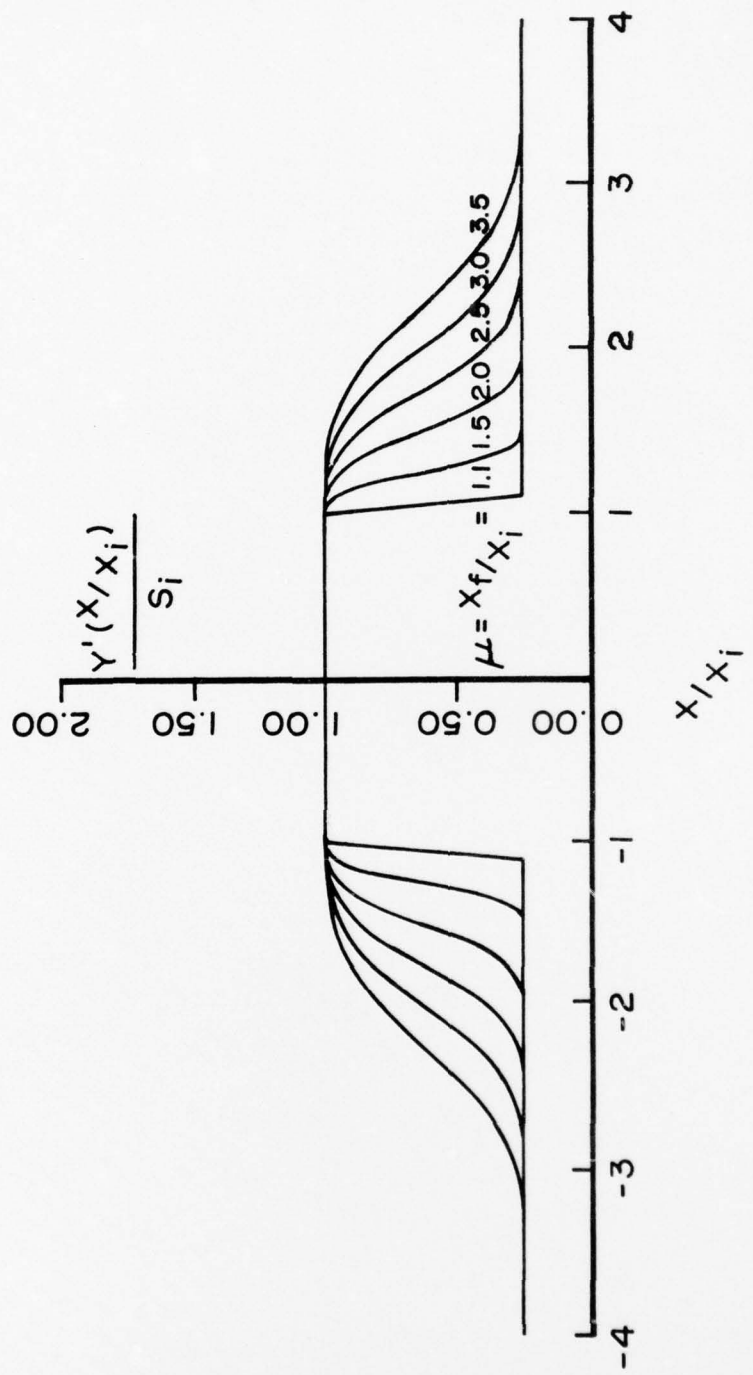


Fig. 7

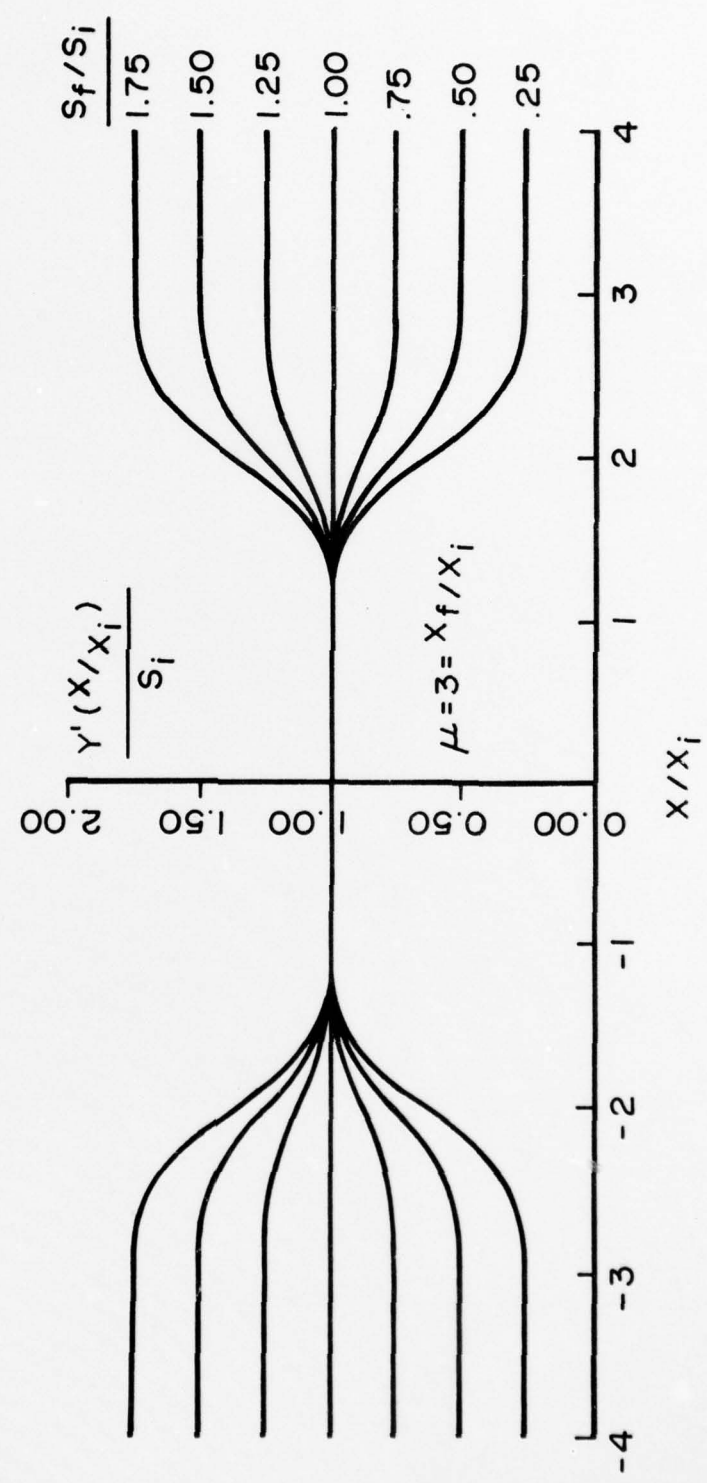


Fig. 8

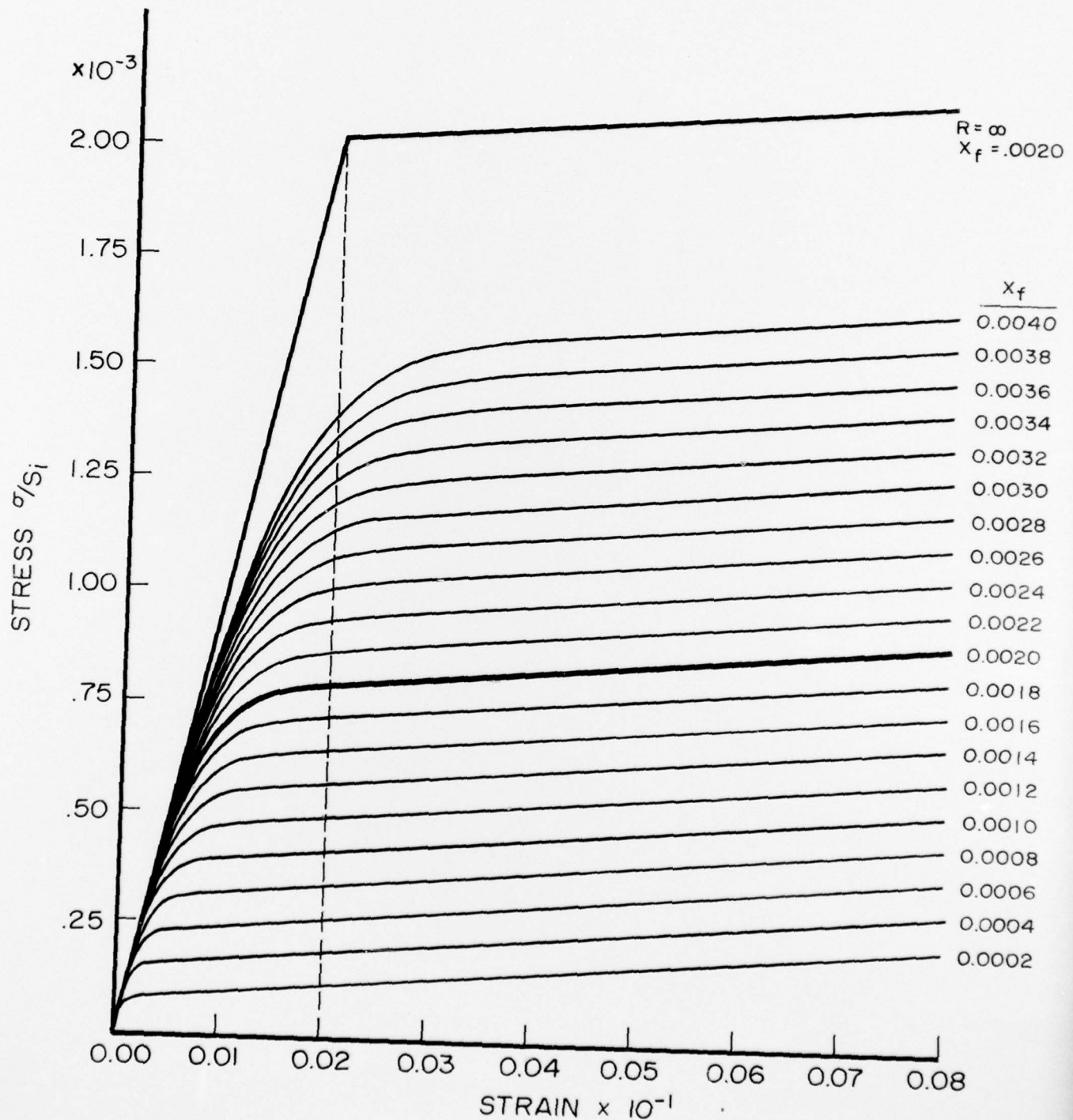


Fig. 9

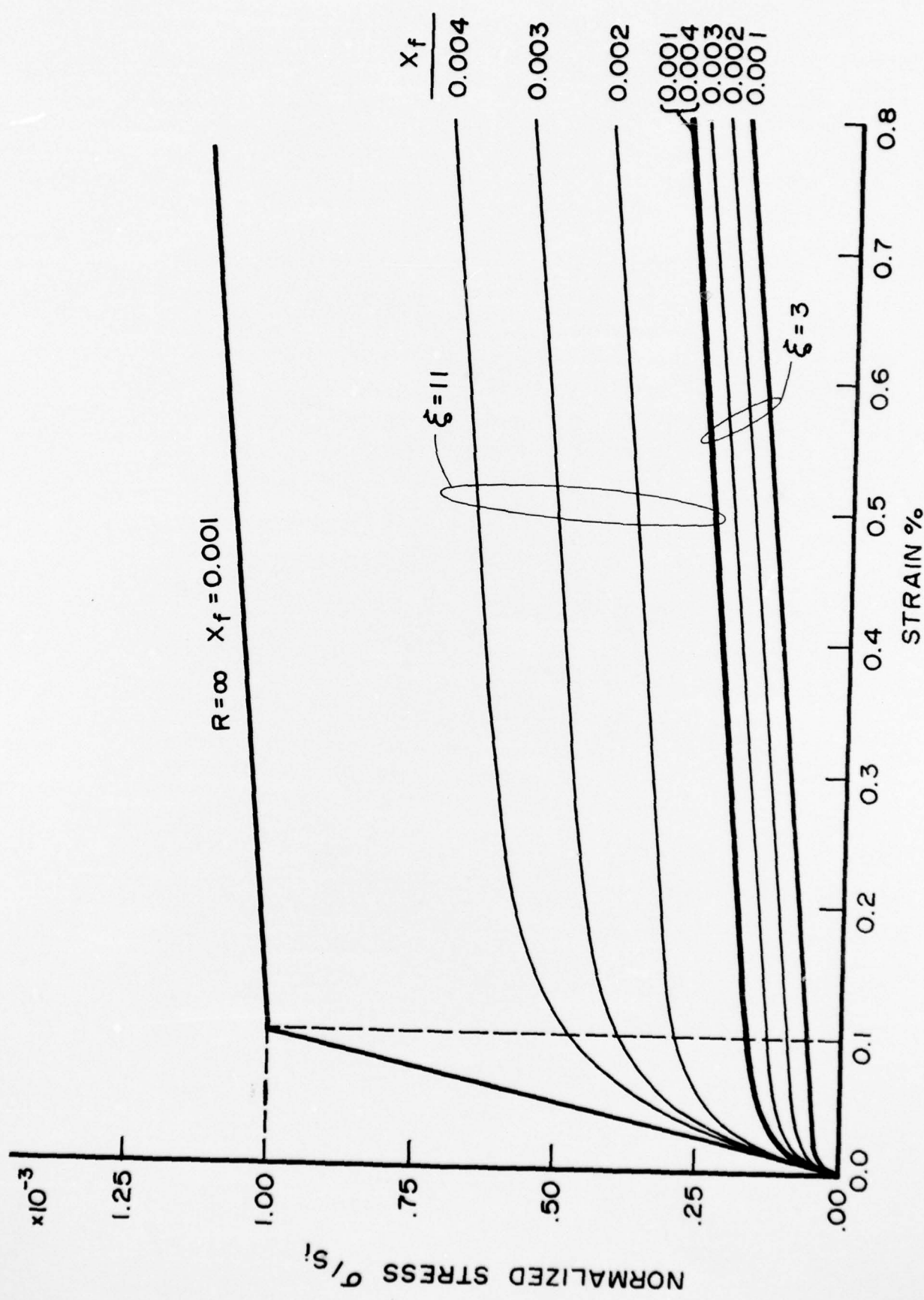
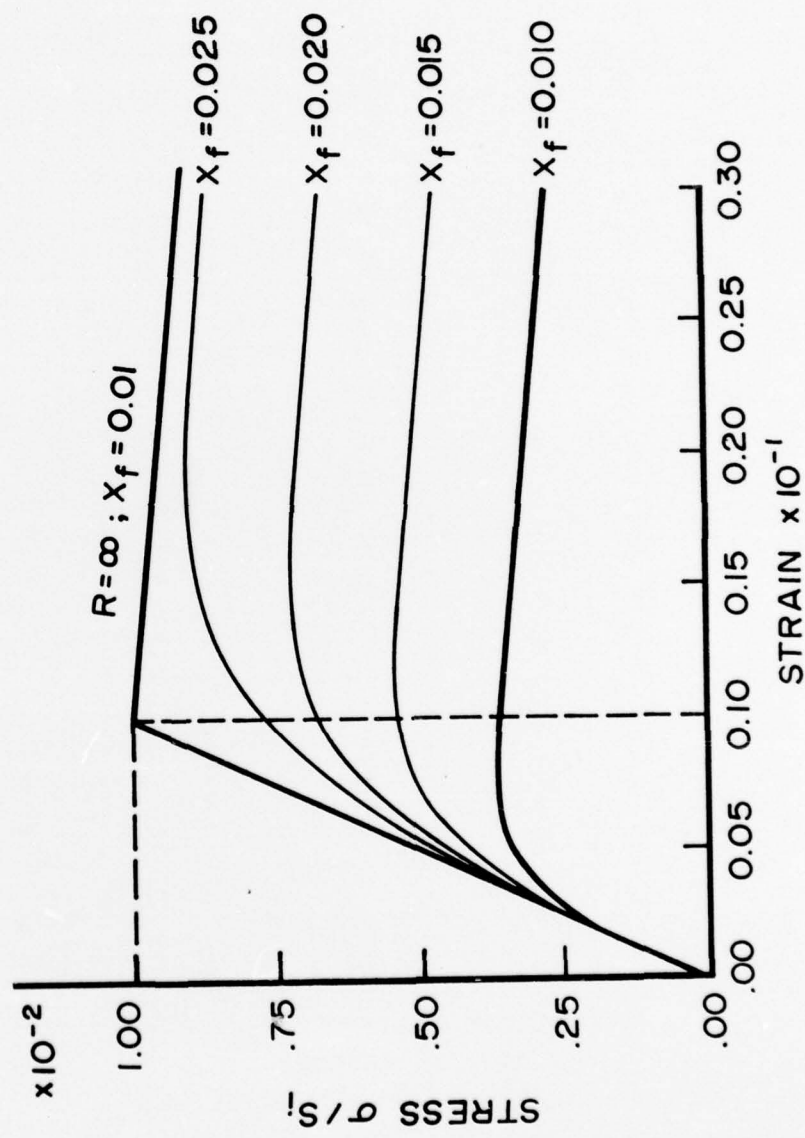


Fig. 10

Fig. 11



PART 1 - GOVERNMENT

Administrative & Liaison Activities

Chief of Naval Research
Department of the Navy
Arlington, Virginia 22217
Attn: Code 474 (2)
471
222

Director
ONR Branch Office
495 Summer Street
Boston, Massachusetts 02210

Director
ONR Branch Office
219 S. Dearborn Street
Chicago, Illinois 60604

Director
Naval Research Laboratory
Attn: Code 2629 (ONRL)
Washington, D.C. 20390 (6)

U.S. Naval Research Laboratory
Attn: Code 2627
Washington, D.C. 20390

Director
ONR - New York Area Office
715 Broadway - 5th Floor
New York, N.Y. 10003

Director
ONR Branch Office
1030 E. Green Street
Pasadena, California 91101

Defense Documentation Center
Cameron Station
Alexandria, Virginia 22314 (12)

Army

Commanding Officer
U.S. Army Research Office Durham
Attn: Mr. J. J. Murray
CRD-AA-IP
Box CM, Duke Station
Durham, North Carolina 27706 2.

Commanding Officer
AMXMR-ATL
Attn: Mr. R. Shea
U.S. Army Materials Res. Agency
Watertown, Massachusetts 02172

Watervliet Arsenal
MAGGS Research Center
Watervliet, New York 12189
Attn: Director of Research

Technical Library

Redstone Scientific Info. Center
Chief, Document Section
U.S. Army Missile Command
Redstone Arsenal, Alabama 35809

Army R&D Center
Fort Belvoir, Virginia 22060

Navy

Commanding Officer and Director
Naval Ship Research & Development Center
Bethesda, Maryland 20034
Attn: Code 042 (Tech. Lib. Br.)
17 (Struc. Mech. Lab.)
172
172
174
177
1800 (Appl. Math. Lab.)
5412S (Dr. W.D. Sette)
19 (Dr. M.M. Sevik)
1901 (Dr. M. Strassberg)
1945
196 (Dr. D Feit)
1962

Naval Weapons Laboratory
Dahlgren, Virginia 22448

Naval Research Laboratory
Washington, D.C. 20375
Attn: Code 8400
8410
8430
8440
6300
6390
6380

Undersea Explosion Research Div.
Naval Ship R&D Center
Norfolk Naval Shipyard
Portsmouth, Virginia 23709
Attn: Dr. E. Palmer
Code 780

Naval Ship Research & Development Center
Annapolis Division
Annapolis, Maryland 21402
Attn: Code 2740 - Dr. Y.F. Wang
28 - Mr. R.J. Wolfe
281 - Mr. R.B. Niederberger
2814 - Dr. H. Vanderveldt

Technical Library
Naval Underwater Weapons Center
Pasadena Annex
3202 E. Foothill Blvd.
Pasadena, California 91107

U.S. Naval Weapons Center
China Lake, California 93557
Attn: Code 4062 - Mr. W. Werback
4520 - Mr. Ken Bischel

Commanding Officer
U.S. Naval Civil Engr. Lab.
Code L31
Port Hueneme, California 93041

Technical Director
U.S. Naval Ordnance Laboratory
White Oak
Silver Spring, Maryland 20910

Technical Director
Naval Undersea R&D Center
San Diego, California 92132

Supervisor of Shipbuilding
U.S. Navy
Newport News, Virginia 23607

Technical Director
Mare Island Naval Shipyard
Vallejo, California 94592

U.S. Navy Underwater Sound Ref. Lab.
Office of Naval Research
P.O. Box 8337
Orlando, Florida 32806

Chief of Naval Operations
Dept. of the Navy
Washington, D.C. 20350
Attn: Code Op07T

Strategic Systems Project Office
Department of the Navy
Washington, D.C. 20390
Attn: NSP-001 Chief Scientist

Deep Submergence Systems
Naval Ship Systems Command
Code 39522
Department of the Navy
Washington, D.C. 20360

Engineering Dept.
U.S. Naval Academy
Annapolis, Maryland 21402

Naval Air Systems Command
Dept. of the Navy
Washington, D.C. 20360
Attn: NAVAIR 5302 Aero & Structures
5308 Structures
52031F Materials
604 Tech. Library
320B Structures
Director, Aero Mechanics
Naval Air Development Center
Johnsville
Warminster, Pennsylvania 18974

Technical Director
U.S. Naval Undersea R&D Center
San Diego, California 92132

Engineering Department
U.S. Naval Academy
Annapolis, Maryland 21402

Naval Facilities Engineering Command
Dept. of the Navy
Washington, D.C. 20360
Attn: NAVFAC 03 Research & Development
04 " "
14114 Tech. Library

Naval Sea Systems Command
Dept. of the Navy
Washington, D.C. 20360
Attn: NAVSHIP 03 Res. & Technology
031 Ch. Scientist for R&D
03412 Hydromechanics
037 Ship Silencing Div.
035 Weapons Dynamics

Naval Ship Engineering Center
Prince George's Plaza
Hyattsville, Maryland 20782

Attn: NAVSEC 6100 Ship Sys Engr & Des Dep
6102C Computer-Aided Ship Des
6105G
6110 Ship Concept Design
6120 Hull Div.
6120D Hull Div.
6128 Surface Ship Struct.
6129 Submarine Struct.

Air Force

Commander WADD
Wright-Patterson Air Force Base
Dayton, Ohio 45433
Attn: Code WWRMDD
AFFDL (FDDDS)
Structures Division
AFLC (MCEEA)

Chief, Applied Mechanics Group
U.S. Air Force Inst. of Tech.
Wright-Patterson Air Force Base
Dayton, Ohio 45433

Chief, Civil Engineering Branch
WLRC, Research Division
Air Force Weapons Laboratory
Kirtland AFB, New Mexico 87117

Air Force Office of Scientific Research
1400 Wilson Blvd.
Arlington, Virginia 22209
Attn: Mechanics Div.

NASA

Structures Research Division
National Aeronautics & Space Admin.
Langley Research Center
Langley Station
Hampton, Virginia 23365

National Aeronautic & Space Admin.
Associate Administrator for Advanced
Research & Technology
Washington, D.C. 02546

Scientific & Tech. Info. Facility
NASA Representative (S-AK/DL)
P.O. Box 5700
Bethesda, Maryland 20014

Other Government Activities

Commandant
Chief, Testing & Development Div.
U.S. Coast Guard
1300 E. Street, N.W.
Washington, D.C. 20226

Technical Director
Marine Corps Dev. & Educ. Command
Quantico, Virginia 22134

Director
National Bureau of Standards
Washington, D.C. 20234
Attn: Mr. B.L. Wilson. EM 219

Dr. M. Gaus
National Science Foundation
Engineering Division
Washington, D.C. 20550

Science & Tech. Division
Library of Congress
Washington, D.C. 20540

Director
Defense Nuclear Agency
Washington, D.C. 20305
Attn: SPSS

Commander Field Command
Defense Nuclear Agency
Sandia Base
Albuquerque, New Mexico 87115

Director Defense Research & Engrg
Technical Library
Room 3C-128
The Pentagon
Washington, D.C. 20301

Chief, Airframe & Equipment Branch
FS-120
Office of Flight Standards
Federal Aviation Agency
Washington, D.C. 20553

Chief, Research and Development
Maritime Administration
Washington, D.C. 20235

Deputy Chief, Office of Ship Constr.
Maritime Administration
Washington, D.C. 20235
Attn: Mr. U.L. Russo

Atomic Energy Commission
Div. of Reactor Devel. & Tech.
Germantown, Maryland 20767

Ship Hull Research Committee
National Research Council
National Academy of Sciences
2101 Constitution Avenue
Washington, D.C. 20418
Attn: Mr. A.R. Lytle

PART 2 - CONTRACTORS AND OTHER
TECHNICAL COLLABORATORS

Universities

Dr. J. Tinsley Oden
University of Texas at Austin
345 Eng. Science Bldg.
Austin, Texas 78712

Prof. Julius Miklowitz
California Institute of Technology
Div. of Engineering & Applied Sciences
Pasadena, California 91109

Dr. Harold Liebowitz, Dean
School of Engr. & Applied Science
George Washington University
725 - 23rd St., N.W.
Washington, D.C. 20006

Prof. Eli Sternberg
California Institute of Technology
Div. of Engr. & Applied Sciences
Pasadena, California 91109

Prof. Paul M. Naghdi
University of California
Div. of Applied Mechanics
Etcheverry Hall
Berkeley, California 94720

Professor P. S. Symonds
Brown University
Division of Engineering
Providence, R.I. 02912

Prof. A. J. Durelli
The Catholic University of America
Civil/Mechanical Engineering
Washington, D.C. 20017

Prof. R.B. Testa
Columbia University
Dept. of Civil Engineering
S.W. Mudd Bldg.
New York, N.Y. 10027

Prof. H. H. Bleich
Columbia University
Dept. of Civil Engineering
Amsterdam & 120th St.
New York, N.Y. 10027

Prof. F.L. DiMaggio
Columbia University
Dept. of Civil Engineering
616 Mudd Building
New York, N.Y. 10027

Prof. A.M. Freudenthal
George Washington University
School of Engineering &
Applied Science
Washington, D.C. 20006

D. C. Evans
University of Utah
Computer Science Division
Salt Lake City, Wash 84112

Prof. Norman Jones
Massachusetts Inst. of Technology
Dept. of Naval Architecture &
Marine Engrng
Cambridge, Massachusetts 02139

Professor Albert I. King
Biomechanics Research Center
Wayne State University
Detroit, Michigan 48202

Dr. V. R. Hodgson
Wayne State University
School of Medicine
Detroit, Michigan 48202

Dean B. A. Boley
Northwestern University
Technological Institute
2145 Sheridan Road
Evanston, Illinois 60201

Prof. P.G. Hodge, Jr.
University of Minnesota
Dept. of Aerospace Engng & Mechanics
Minneapolis, Minnesota 55455

Dr. D.C. Drucker
University of Illinois
Dean of Engineering
Urbana, Illinois 61801

Prof. N.M. Newmark
University of Illinois
Dept. of Civil Engineering
Urbana, Illinois 61801

Prof. E. Reissner
University of California, San Diego
Dept. of Applied Mechanics
La Jolla, California 92037

Prof. William A. Nash
University of Massachusetts
Dept. of Mechanics & Aerospace Engng.
Amherst, Massachusetts 01002

Library (Code 0384)
U.S. Naval Postgraduate School
Monterey, California 93940

Prof. Arnold Allentuch
Newark College of Engineering
Dept. of Mechanical Engineering
323 High Street
Newark, New Jersey 07102

Dr. George Herrmann
Stanford University
Dept. of Applied Mechanics
Stanford, California 94305

Prof. J. D. Achenbach
Northwestern University
Dept. of Civil Engineering
Evanston, Illinois 60201

Director, Applied Research Lab.
Pennsylvania State University
P. O. Box 30
State College, Pennsylvania 16801

Prof. Eugen J. Skudrzyk
Pennsylvania State University
Applied Research Laboratory
Dept. of Physics - P.O. Box 30
State College, Pennsylvania 16801

Prof. J. Kempner
Polytechnic Institute of Brooklyn
Dept. of Aero. Engrg. & Applied Mech
333 Jay Street
Brooklyn, N.Y. 11201

Prof. J. Klosner
Polytechnic Institute of Brooklyn
Dept. of Aerospace & Appl. Mech.
333 Jay Street
Brooklyn, N.Y. 11201

Prof. R.A. Schapery
Texas A&M University
Dept. of Civil Engineering
College Station, Texas 77840

Prof. W.D. Pilkey
University of Virginia
Dept. of Aerospace Engineering
Charlottesville, Virginia 22903

Dr. H.G. Schaeffer
University of Maryland
Aerospace Engineering Dept.
College Park, Maryland 20742

Prof. K.D. Willmert
Clarkson College of Technology
Dept. of Mechanical Engineering
Potsdam, N.Y. 13676

Dr. J.A. Stricklin
Texas A&M University
Aerospace Engineering Dept.
College Station, Texas 77843

Dr. L.A. Schmit
University of California, LA
School of Engineering & Applied Science
Los Angeles, California 90024

Dr. H.A. Kamel
The University of Arizona
Aerospace & Mech. Engineering Dept.
Tucson, Arizona 85721

Dr. B.S. Berger
University of Maryland
Dept. of Mechanical Engineering
College Park, Maryland 20742

Prof. G. R. Irwin
Dept. of Mechanical Engrg.
University of Maryland
College Park, Maryland 20742

Dr. S.J. Fenves
Carnegie-Mellon University
Dept. of Civil Engineering
Schenley Park
Pittsburgh, Pennsylvania 15213

Dr. Ronald L. Huston
Dept. of Engineering Analysis
Mail Box 112
University of Cincinnati
Cincinnati, Ohio 45221

Prof. George Sih
Dept. of Mechanics
Lehigh University
Bethlehem, Pennsylvania 18015

Prof. A.S. Kobayashi
University of Washington
Dept. of Mechanical Engineering
Seattle, Washington 98105

Librarian
Webb Institute of Naval Architecture
Crescent Beach Road, Glen Cove
Long Island, New York 11542

Prof. Daniel Frederick
Virginia Polytechnic Institute
Dept. of Engineering Mechanics
Blacksburg, Virginia 24061

Prof. A.C. Eringen
Dept. of Aerospace & Mech. Sciences
Princeton University
Princeton, New Jersey 08540

Dr. S.L. Koh
School of Aero., Astro. & Engr. Sc.
Purdue University
Lafayette, Indiana 47907

Prof. E.H. Lee
Div. of Engrg. Mechanics
Stanford University
Stanford, California 94305

Prof. R.D. Mindlin
Dept. of Civil Engrg.
Columbia University
S.W. Mudd Building
New York, N.Y. 10027

Prof. S.B. Dong
University of California
Dept. of Mechanics
Los Angeles, California 90024
Prof. Burt Paul
University of Pennsylvania
Towne School of Civil & Mech. Engrg.
Rm. 113 - Towne Building
220 S. 33rd Street
Philadelphia, Pennsylvania 19104
Prof. H.W. Liu
Dept. of Chemical Engr. & Metal.
Syracuse University
Syracuse, N.Y. 13210

Prof. S. Bodner
Technion R&D Foundation
Haifa, Israel

Prof. R.J.H. Bolland
Chairman, Aeronautical Engr. Dept.
207 Guggenheim Hall
University of Washington
Seattle, Washington 98105

Prof. G.S. Heller
Division of Engineering
Brown University
Providence, Rhode Island 02912

Prof. Werner Goldsmith
Dept. of Mechanical Engineering
Div. of Applied Mechanics
University of California
Berkeley, California 94720

Prof. J.R. Rice
Division of Engineering
Brown University
Providence, Rhode Island 02912

Prof. R.S. Rivlin
Center for the Application of Mathematics
Lehigh University
Bethlehem, Pennsylvania 18015

Library (Code 0384)
U.S. Naval Postgraduate School
Monterey, California 93940

Dr. Francis Cozzarelli
Div. of Interdisciplinary
Studies & Research
School of Engineering
State University of New York
Buffalo, N.Y. 14214

Industry and Research Institutes

Library Services Department
Report Section Bldg. 14-14
Argonne National Laboratory
9700 S. Cass Avenue
Argonne, Illinois 60440

Dr. R.C. DeHart
Southwest Research Institute
Dept. of Structural Research
P.O. Drawer 28510
San Antonio, Texas 78284

Dr. M. C. Junger
Cambridge Acoustical Associates
129 Mount Auburn St.
Cambridge, Massachusetts 02138

Dr. M.L. Baron
Weidlinger Associates,
Consulting Engineers
110 East 59th Street
New York, N.Y. 10022

Dr. L.H. Chen
General Dynamics Corporation
Electric Boat Division
Groton, Connecticut 06340

Dr. W.A. von Riesemann
Sandia Laboratories
Sandia Base
Albuquerque, New Mexico 87115

Dr. J.E. Greenspon
J.G. Engineering Research Associates
3831 Menlo Drive
Baltimore, Maryland 21215

Dr. T.L. Geers
Lockheed Missiles & Space Co.
Palo Alto Research Laboratory
3251 Hanover Street
Palo Alto, California 94304

Dr. S. Batdorf
The Aerospace Corp.
P.O. Box 92957
Los Angeles, California 90009

Dr. J.L. Tocher
Boeing Computer Services, Inc.
P.O. Box 24346
Seattle, Washington 98124

Dr. K.C. Park
Lockheed Palo Alto Research Laboratory
Dept. 5233, Bldg. 205
3251 Hanover Street
Palo Alto, CA 94304

Mr. Willian Caywood
Code BBE, Applied Physics Laboratory
8621 Georgia Avenue
Silver Spring, Maryland 20034

Library
Newport News Shipbuilding &
Dry Dock Company
Newport News, Virginia 23607

Mr. P.C. Durup
Lockheed-California Company
Aeromechanics Dept., 74-43
Burbank, California 91503

Dr. W.F. Bozich
McDonnell Douglas Corporation
5301 Bolsa Ave.
Huntington Beach, CA 92647

Dr. H.N. Abramson
Southwest Research Institute
Technical Vice President
Mechanical Sciences
P.O. Drawer 28510
San Antonio, Texas 78284

Unclassified

SECURITY CLASSIFICATION OF THIS PAGE (When Data Entered)

REPORT DOCUMENTATION PAGE		READ INSTRUCTIONS BEFORE COMPLETING FORM
1. REPORT NUMBER 14 RPI-CS-77-1	2. GOVT ACCESSION NO.	3. RECIPIENT'S CATALOG NUMBER 9
4. TITLE (and Subtitle) Nonlinear Monotonic Functions with Selectable Intervals of Almost Constant or Linear Behavior with Application to Total Strain Viscoplasticity.		5. TYPE OF REPORT & PERIOD COVERED Topical Report
6. AUTHOR(s) E.P. Cernocky and E. Krempel		7. PERFORMING ORG. REPORT NUMBER 10 N00014-76-C-0231 new
8. CONTRACT OR GRANT NUMBER(s) 15		9. PERFORMING ORGANIZATION NAME AND ADDRESS Department of Mechanical Engineering, Aeronautical Engineering & Mechanics Rensselaer Polytechnic Institute, Troy, NY 12181
10. PROGRAM ELEMENT, PROJECT, TASK AREA & WORK UNIT NUMBERS NR 064-571		11. CONTROLLING OFFICE NAME AND ADDRESS Dept. of the Navy, Office of Naval Research Structural Mechanics Program Arlington, Va. 22217
12. REPORT DATE 11 January 1977		13. NUMBER OF PAGES 123
14. MONITORING AGENCY NAME & ADDRESS (if different from Controlling Office) Office of Naval Research - Resident Representative 715 Broadway - 5th Floor New York, NY 10003		15. SECURITY CLASS. (of this report) Unclassified
16. DISTRIBUTION STATEMENT (of this Report) Approved for public release; distribution unlimited.		
17. DISTRIBUTION STATEMENT (of the abstract entered in Block 20, if different from Report)		
18. SUPPLEMENTARY NOTES		
19. KEY WORDS (Continue on reverse side if necessary and identify by block number) Plasticity, viscoplasticity, cyclic loading, rate effects, analytic modelling, numerical experiments, curve fitting of mechanical behavior data.		
20. ABSTRACT (Continue on reverse side if necessary and identify by block number) A rather general method is given to construct classes of functions with an arbitrary almost constant (linear) initial interval followed by a non-prescribed interval of monotonic nonlinear behavior. This region of nonlinear behavior is succeeded by an unbounded interval of almost constant (linear) behavior. They contain not more than four selectable parameters and are synthesized from analytic, monotonic, normalized and bounded base functions through the introduction of two separate kernel sets, subsequent addition and next page		

Unclassified

SECURITY CLASSIFICATION OF THIS PAGE(When Data Entered)

cont.

integration. As examples we give the special functions based on the error, the hyperbolic tangent, the inverse tangent, a rational and the incomplete gamma function. Limiting function forms, such as the bilinear form, are derived for limiting values of the parameters.

We have found these functions useful in the total strain approach to viscoplasticity, i.e., the analytical modelling of stress-strain diagrams, strain (stress)-rate effects, creep and relaxation curves for monotonic and cyclic loading. Also these functions offer great flexibility in the curve fitting of experimental data generated in the above-mentioned tests.



Unclassified

SECURITY CLASSIFICATION OF THIS PAGE(When Data Entered)